J Eng Math (2006) 56:385–413
DOI 10.1007/s10665-006-9046-1

ORIGINAL ARTICLE

# Optimal-control methods for two new classes of smart obstacles in time-dependent acoustic scattering

**Lorella Fatone · Graziella Pacelli · Maria Cristina Recchioni · Francesco Zirilli**

Received: 15 September 2004 / Accepted: 18 March 2006 /
Published online: 13 September 2006


**Abstract** Time-dependent acoustic scattering problems involving "smart" obstacles are considered. When hit by an incident acoustic field, smart obstacles react in an attempt to pursue a preassigned goal. Let $\mathbb{R}^3$ be the three-dimensional real Euclidean space, and let $\Omega \subset \mathbb{R}^3$ be a bounded simply connected open set with a Lipschitz boundary characterized by a constant acoustic boundary impedance $\chi$, immersed in an isotropic and homogeneous medium that fills $\mathbb{R}^3 \backslash \Omega$. The closure of $\Omega$ will be denoted as $\overline{\Omega}$. When hit by an incident field, the obstacle $\Omega$ pursues the preassigned goal through the action of a control input acting on its boundary (i.e., a quantity with dimensions of a pressure divided by a time). The obstacles considered in this paper monitor the control input acting on their boundaries in order to achieve one of the following goals: (i) be furtive in a given set of the frequency space, and (ii) appear in a given set of the frequency space and outside a given set of $\mathbb{R}^3$ containing $\Omega$ and $\Omega_G$ as similar as possible to a "ghost" obstacle $\Omega_G$ having boundary acoustic impedance $\chi_G$. It is assumed that $\overline{\Omega} \cap \overline{\Omega}_G = \emptyset$ and $\Omega_G \neq \emptyset$. The problem corresponding to the first goal will be called the definite-band furtivity problem, and the problem corresponding to the second goal will be called the definite-band ghost-obstacle problem. These two

L. Fatone
Dipartimento di Matematica Pura e Applicata, Università di Modena e Reggio Emilia,
Via Campi 213/b, 41100 Modena, Italy
e-mail: fatone.lorella@unimo.it

G. Pacelli · M. C. Recchioni
Dipartimento di Scienze Sociali "D. Serrani", Università Politecnica delle Marche,
Piazza Martelli 8, 60121 Ancona, Italy

G. Pacelli
e-mail: g.pacelli@univpm.it

M. C. Recchioni
e-mail: m.c.recchioni@univpm.it

F. Zirilli (✉)
Dipartimento di Matematica "G. Castelnuovo",
Università di Roma "La Sapienza",
Piazzale Aldo Moro 2, 00185 Roma, Italy
e-mail: f.zirilli@caspur.it

goals define two classes of smart obstacles. In this paper, these problems are modeled as optimal-control problems for the wave equation introducing a control input acting on the boundary of $\Omega$ for time $t \in \mathbb{R}$. The cost functionals proposed depend on the value of the control input on the boundary of the obstacle and on the value of the scattered acoustic field generated by the obstacle on the boundary in the "furtivity case", and on the boundary of a suitable set containing $\Omega$ and $\Omega_G$ in the "ghost-obstacle case". Under some assumptions, the use of the Pontryagin maximum principle allows us to formulate the first-order optimality conditions for the definite-band furtivity problem and for the definite-band ghost-obstacle problem as exterior problems outside the obstacle for a system of two coupled wave equations. Numerical methods to solve these exterior problems are developed by extending previous work. These methods belong to the class of the operator-expansion methods that are highly parallelizable. Numerical experiments proving the validity of the control problems proposed as mathematical models of the definite-band furtivity problem and definite-band ghost obstacle problem are presented. The numerical results obtained with a parallel implementation of the numerical methods developed are discussed and their properties are established. The speed-up factors obtained using parallel computing are really impressive. The website: *http://www.econ.univpm.it/recchioni/w11* contains animations and virtual reality applications relative to the numerical experiments.

**Keywords** Acoustic obstacle scattering · Open-loop control · Operator-expansion method · Smart obstacles

## 1 Introduction

When illuminated by an incoming field, smart or active obstacles react by actuating a policy in order to pursue an assigned goal. The development and dissemination of recent innovations in sensors, electronic chips, and actuators have made possible the realization of smart objects in many practical situations. Applications of smart objects range from cutting-edge military applications to everyday life devices such as, for example, washing machines. The design and realization of smart objects can be improved by the availability of satisfactory mathematical models that describe their behavior. The general mathematical model we have in mind to describe the behavior of a smart object is an optimal-control problem involving ordinary and/or partial differential equations. In recent papers, the authors and coworkers have studied smart obstacles in the context of acoustic and electromagnetic scattering. In these contexts, the smart obstacles considered circulate suitable control inputs on their boundaries in order to pursue their goals. The goal of the smart obstacles studied is one of the following:

(1) To be undetectable (i.e., furtivity problem) [1–3].
(2) To appear with a shape and a boundary impedance different from the actual ones (i.e., masking problem) [2–4].
(3) To appear in a location in space different from its actual one, eventually with a shape and boundary impedance different from its actual ones (i.e., ghost obstacle problem) [5].

The optimal-control problems associated with these classes of obstacles provide a way of characterizing and computing the control variable (i.e., pressure divided by time) as the optimal solution of the mathematical problems considered.

A possible physical device to build an actuator for these control variables could be a set of pistons located on the boundary of the obstacle. The pistons should act creating either a compression or a decompression in the medium surrounding the obstacle in contact with the boundary according to the values of the control variable. The distance traveled by the pistons should be negligible compared to the size of the obstacle, that is, significant deformation of the boundary of the obstacle must be avoided.

In this paper, we introduce certain new classes of smart obstacles that pursue one of the previous goals restricted to a definite band in the frequency space. For the sake of brevity, we restrict our analysis to the

definite-band furtivity problem and to the definite-band ghost-obstacle problem in the acoustic case. These problems are formulated as optimal-control problems for the wave equation. The acoustic definite-band masking problem can be treated similarly. We consider the study of these problems as a preliminary to the study of the corresponding problems in the electromagnetic case where the wave equation is replaced by the Maxwell equations.

The definite-band problems are of great interest in practical situations. For example, they are of great interest in the design and implementation of smart radar absorbers. Smart radar absorbers are a key ingredient of several devices used in the aerospace industry. In the past, radar absorbers have been designed using one of the following ideas to achieve the absorbing effect, including destructive inference (for example in the so-called Salisbury screen and in the Jaumann stack), and by absorbing and converting the incident energy into heat (for example in the Dallenbach layer). Recently, phase-switched screens have been introduced as tools to build radar absorbers (e.g., [6–9]). When a phase-switched screen is used, the incident energy is not absorbed but shifted in frequency, using phase modulation so that any reflected energy falls outside the receiver bandwidth and is thus not detected. Roughly speaking, a phase-switched screen in the terminology of this paper is a smart object that in the electromagnetic case pursues the goal of: "definite-band furtivity". This example shows the relevance of the definite-band furtivity problem in the acoustic case.

Restricting the goal pursued to a definite band in the frequency space, as proposed in this paper, modifies substantially the mathematical formulation of the problems under consideration. In fact, the optimal-control problems used to model problems (1–3), in particular, the cost functionals that must be minimized in order to achieve the goal over the entire frequency space, must be reconsidered in order to model appropriately the problem formulated only on the desired band in the frequency space. The presence of the definite band necessitates the use of suitable convolutions involving the inverse Fourier transform of the characteristic function of the definite frequency band in the definition of the cost functional (see formulae (8), (9)). Consequently, the first-order optimality conditions of these new optimal-control problems change substantially and cannot be deduced from those derived in [1, 4, 5] for the optimal-control problems (1)–(3). That is, the first-order optimality conditions are not expressed by two wave equations coupled by local boundary conditions as in [1, 4, 5], but the coupling between the two wave equations is given by non-local (in time) boundary conditions (see Eq. (22)). As a consequence, the way of solving the first-order optimality conditions must be changed.

### 1.1 Mathematical formulation of the definite-band ghost-obstacle problem

Let $\mathbb{R}$ be the set of real numbers, $\mathbb{R}^3$ be the three-dimensional real Euclidean space, and $\underline{x} = (x_1, x_2, x_3)^{\mathrm{T}} \in \mathbb{R}^3$ be a generic vector, where the superscript T denotes the transpose. We denote with $(\cdot,\cdot)$ the Euclidean scalar product in $\mathbb{R}^3$, and with $\|\cdot\|$ the corresponding Euclidean vector norm.

We now describe the data defining the definite-band furtivity and the definite-band ghost-obstacle problems. Let $\Omega \subset \mathbb{R}^3$, $\Omega_G \subset \mathbb{R}^3$ be two bounded simply connected open sets with locally Lipschitz boundaries $\partial\Omega$, $\partial\Omega_G$, and let $\overline{\Omega}$ and $\overline{\Omega}_G$ be their closures, respectively. We denote with $\underline{n}(\underline{x}) = (n_1(\underline{x}), n_2(\underline{x}), n_3(\underline{x}))^T \in \mathbb{R}^3$, $\underline{x} \in \partial\Omega$ the outward unit normal vector to $\partial\Omega$. Since $\Omega$ has a locally Lipschitz boundary, $\underline{n}(\underline{x})$, $\underline{x} \in \partial\Omega$, exists almost everywhere (see [10, Lemma 2.42, p. 88]); similar statements hold for the outward unit normal vector to $\partial\Omega_G$. Furthermore, $\Omega_G$ is such that $\Omega_G \neq \emptyset$ and $\overline{\Omega} \cap \overline{\Omega}_G = \emptyset$. We assume that $\Omega$ and $\Omega_G$ are characterized by acoustic constant boundary impedances $\chi$, $\chi \geq 0$, and $\chi_G$, $\chi_G \geq 0$, respectively. The case $\chi = +\infty$ and/or $\chi_G = +\infty$ (i.e., the case of acoustically hard obstacles) can be treated with simple modifications of the formulae presented in this paper. We refer to $(\Omega; \chi)$ as the obstacle, and to $(\Omega_G; \chi_G)$ as the ghost obstacle. Without loss of generality, we can assume that the origin of the coordinate system lies in $\Omega$. We note that the last assumption implies that there exists $a > 0$ such that the closed sphere with center at the origin and radius $a$ is contained in $\Omega$, i.e.: $\overline{B}_a = \{\underline{x} \in \mathbb{R}^3 \mid \|\underline{x}\| \leq a\} \subset \Omega$. Let $K \subset \mathbb{R}$ be an open

set, symmetric with respect to the origin, chosen as the band in the frequency space where the goal of the furtivity problem or of the ghost-obstacle problem must be pursued. The assumption that $K$ is symmetric with respect to the origin is made to keep the exposition simple and can be easily removed. We consider an acoustic incident wave $u^i(\underline{x},t)$, $(\underline{x},t) \in \mathbb{R}^3 \times \mathbb{R}$, propagating in a homogeneous isotropic medium at equilibrium, with no source terms present, satisfying the wave equation with wave propagation velocity $c > 0$ in $\mathbb{R}^3 \times \mathbb{R}$. Finally, we denote with $u^s(\underline{x},t)$, $(\underline{x},t) \in (\mathbb{R}^3 \setminus \overline{\Omega}) \times \mathbb{R}$, and with $u^s_G(\underline{x},t)$, $(\underline{x},t) \in (\mathbb{R}^3 \setminus \overline{\Omega_G}) \times \mathbb{R}$ the waves scattered, respectively, by the obstacle $(\Omega;\chi)$ and by the ghost obstacle $(\Omega_G;\chi_G)$ when hit by $u^i(\underline{x},t)$, $(\underline{x},t) \in \mathbb{R}^3 \times \mathbb{R}$.

The scattered acoustic field $u^s(\underline{x},t)$, $(\underline{x},t) \in (\mathbb{R}^3 \setminus \overline{\Omega}) \times \mathbb{R}$ is defined as the solution of the following exterior problem for the wave equation (see [11]):

$$\triangle u^s(\underline{x},t) - \frac{1}{c^2}\frac{\partial^2 u^s}{\partial t^2}(\underline{x},t) = 0, \quad (\underline{x},t) \in (\mathbb{R}^3 \setminus \overline{\Omega}) \times \mathbb{R} \tag{1}$$

with the boundary condition (see [12, p. 66]):

$$-\frac{\partial u^s}{\partial t}(\underline{x},t) + c\chi \frac{\partial u^s}{\partial \underline{n}(\underline{x})} = g(\underline{x},t), \quad (\underline{x},t) \in \partial\Omega \times \mathbb{R}, \tag{2}$$

where $g(\underline{x},t)$ is given by

$$g(\underline{x},t) = \frac{\partial u^i}{\partial t}(\underline{x},t) - c\chi \frac{\partial u^i}{\partial \underline{n}(\underline{x})}(\underline{x},t), \quad (\underline{x},t) \in \partial\Omega \times \mathbb{R}, \tag{3}$$

the condition at infinity

$$u^s(\underline{x},t) = O\left(\frac{1}{r}\right), \quad r \to +\infty,\ t \in \mathbb{R}, \tag{4}$$

and the radiation condition

$$\frac{\partial u^s}{\partial r}(\underline{x},t) + \frac{1}{c}\frac{\partial u^s}{\partial t}(\underline{x},t) = o\left(\frac{1}{r}\right), \quad r \to +\infty,\ t \in \mathbb{R}, \tag{5}$$

where $r = \|\underline{x}\|$, $\underline{x} \in \mathbb{R}^3$, $\triangle = \sum_{i=1}^3 \frac{\partial^2}{\partial x_i^2}$ is the Laplacian operator, $c > 0$ is the wave propagation velocity, and $O(\cdot)$ and $o(\cdot)$ are the Landau symbols. We note that $g(\underline{x},t)$, $(\underline{x},t) \in \partial\Omega \times \mathbb{R}$ is defined almost everywhere, and the boundary condition (2) can be adapted to deal with the limiting case of acoustically hard obstacles, i.e., $\chi = +\infty$ (see [1, 11]). The obstacle $(\Omega;\chi)$ that scatters the field $u^s$ solution of (1), (2), (4), (5) is called a passive obstacle. The field $u^s_G(\underline{x},t)$, $(\underline{x},t) \in (\mathbb{R}^3 \setminus \overline{\Omega}_G) \times \mathbb{R}$ scattered by the (passive) ghost obstacle is defined as the solution of (1), (2), (4), (5) when in the problem defined above we replace $\Omega$ with $\Omega_G$ and $\chi$ with $\chi_G$. Note that we always consider the ghost obstacle as a passive obstacle.

Let $\omega$ be the conjugate variable of $t$ in the Fourier transform. We consider the following problems:

*Definite-Band Furtivity Problem:* Given an incoming acoustic field $u^i(\underline{x},t)$, $(\underline{x},t) \in \mathbb{R}^3 \times \mathbb{R}$, an obstacle $(\Omega;\chi)$ and an open set $K \subset \mathbb{R}$ symmetric with respect to the origin, choose a suitable control function acting on $\partial\Omega$ for $t \in \mathbb{R}$ so that the Fourier transform with respect to time of the wave scattered by $(\Omega;\chi)$ when hit by the incoming acoustic field $u^i$ is "as small as possible" for $\omega \in K$.

*Definite-Band Ghost Obstacle Problem:* Given an incoming acoustic field $u^i(\underline{x},t)$, $(\underline{x},t) \in \mathbb{R}^3 \times \mathbb{R}$, an obstacle $(\Omega;\chi)$, a ghost obstacle $(\Omega_G;\chi_G)$ and an open set $K \subset \mathbb{R}$ symmetric with respect to the origin, choose a suitable control function acting on $\partial\Omega$ for $t \in \mathbb{R}$ so that the Fourier transform with respect to time of the wave scattered by $(\Omega;\chi)$ when hit by the incoming acoustic field $u^i$ appears outside a given set containing $\Omega$ and $\Omega_G$ and for $\omega \in K$ "as similar as possible" to the Fourier transform of the wave scattered in the same circumstances by the ghost obstacle $(\Omega_G;\chi_G)$.

Note that the physical dimension of the control function is pressure divided by time.

Obstacles that behave according to the requirements of the definite-band furtivity and of the definite-band ghost-obstacle problems are "smart", in the sense that they try to pursue a preassigned goal (i.e.: they try to appear in the region $K$ of the frequency space different from what they are). In fact, the obstacle that hosts on its boundary the control-function solution of the definite-band furtivity problem generates a scattered wave whose Fourier transform with respect to time is "small" when $\omega \in K$. That is, the obstacle reacts trying to be undetectable in the frequency band $K$. The obstacle that hosts on its boundary the control-function solution of the definite-band ghost obstacle problem generates a scattered wave whose Fourier transform with respect to time in the frequency band $K$ resembles outside a given set containing $\Omega$ and $\Omega_G$ the Fourier transform with respect to time of the wave scattered by $(\Omega_G; \chi_G)$.

For simplicity, we now formulate the mathematical model of the definite-band ghost-obstacle problem; later, we will show how to modify this model in order to obtain the mathematical model of the definite-band furtivity problem.

Our goal is to model the definite-band ghost-obstacle problem as an optimal-control problem introducing a control variable $\psi(\underline{x}, t)$, $(\underline{x}, t) \in \partial\Omega \times \mathbb{R}$ acting on the boundary of the obstacle. Toward this aim, we replace the boundary condition (2) with the following boundary condition:

$$-\frac{\partial u^s}{\partial t}(\underline{x}, t) + c\chi \frac{\partial u^s}{\partial \underline{n}(\underline{x})} = g(\underline{x}, t) + (1 + \chi)\psi(\underline{x}, t), \quad (\underline{x}, t) \in \partial\Omega \times \mathbb{R}. \tag{6}$$

Let $\Omega_\epsilon$ be a bounded simply connected open set containing $\Omega$ and $\Omega_G$ with Lipschitz boundary $\partial\Omega_\epsilon$ and let $\mathrm{d}s_{\partial\Omega_\epsilon}$, $\mathrm{d}s_{\partial\Omega}$ be the surface measures on $\partial\Omega_\epsilon$ and $\partial\Omega$ (see [10, Lemma 1.1, pp. 119–120]), respectively. Moreover, let $I_k(\omega)$, $\omega \in \mathbb{R}$, be the characteristic function of the set $K$, that is:

$$I_k(\omega) = \begin{cases} 1, & \omega \in K, \\ 0, & \omega \in \mathbb{R} \setminus K \end{cases} \tag{7}$$

and let $\check{I}_K(t)$, $t \in \mathbb{R}$ be its inverse Fourier transform, and $C_{K,u^s,u^s_G}$ be the following function:

$$C_{K,u^s,u^s_G}(\underline{x}, t) = \int_{\mathbb{R}} \mathrm{d}\tau \; \check{I}_K(\tau)(u^s(\underline{x}, t - \tau) - u^s_G(\underline{x}, t - \tau)), \quad (\underline{x}, t) \in \partial\Omega_\epsilon \times \mathbb{R}. \tag{8}$$

We note that, since $K$ is symmetric with respect to the origin, the function $\check{I}_K$ is real.

We choose the following cost functional:

$$F_{\lambda,\mu,\epsilon}(\psi) = \int_{\mathbb{R}} \mathrm{d}t \left\{ \int_{\partial\Omega_\epsilon} (1 + \chi)\lambda \, C^2_{K,u^s,u^s_G}(\underline{x}, t)\mathrm{d}s_{\partial\Omega_\epsilon} + \int_{\partial\Omega} (1 + \chi)\mu\varsigma\psi^2(\underline{x}, t)\mathrm{d}s_{\partial\Omega} \right\}, \tag{9}$$

where $\lambda \geq 0$, $\mu \geq 0$ are dimensionless constants such that $\lambda + \mu = 1$, and $\varsigma$ is a non-zero positive dimensional constant. We model the definite-band ghost-obstacle problem via the following optimal control problem:

$$\min_{\psi \in \mathrm{C}} F_{\lambda,\mu,\epsilon}(\psi), \tag{10}$$

subject to constraints (1), (4)–(6). The set C lies the space of the admissible controls and will be defined later. The obstacle $(\Omega; \chi)$ that generates the scattered field $u^s$ solution of (10), (1), (4)–(6) is called a smart or active obstacle.

As shown in [1], the cases $\mu = 0$ and $\mu = 1$ are trivial. We choose the cost functional (9) since, when $0 < \mu < 1$, we have $\lambda > 0$, that is, the minimization of $F_{\lambda,\mu,\epsilon}$ reduces the difference between the Fourier transform of the wave $u^s$ scattered by the smart obstacle $(\Omega; \chi)$ and the Fourier transform of the wave $u^s_G$ scattered by the ghost $(\Omega_G; \chi_G)$ on the surface $\partial\Omega_\epsilon$ when $\omega \in K$. As a consequence of this difference remaining small in $\mathbb{R}^3 \setminus \Omega_\epsilon$, an observer located in $\mathbb{R}^3 \setminus \overline{\Omega}_\epsilon$ in the frequency band $K$ observes a scattered field generated by the smart obstacle that resembles the scattered field generated by the ghost, that is, the observer located in $\mathbb{R}^3 \setminus \overline{\Omega}_\epsilon$ that observes the scattered field in the frequency band $K$ is made to believe that the obstacle generating the scattered field is indeed the ghost obstacle. Moreover, due to the second

addendum in (9), minimizing $F_{\lambda,\mu,\epsilon}$ when $0 < \mu < 1$ means also minimizing the "magnitude" of the control function $\psi$ employed. From now on, we restrict our attention to the case $0 < \mu < 1$.

We say that a functional associated with the boundary condition (6) is "local" when it depends only on the values on the boundary of $\Omega$ of the "state variables" $u^s(\underline{x},t)$, $(\underline{x},t) \in \partial\Omega \times \mathbb{R}$ and of the "control variables" $\psi(\underline{x},t)$, $(\underline{x},t) \in \partial\Omega \times \mathbb{R}$. Note that the functional $F_{\lambda,\mu,\epsilon}$ given in (9) is "non-local" with respect to the state variables since it depends on the values of $u^s(\underline{x},t)$, $(\underline{x},t) \in \partial\Omega_\epsilon \times \mathbb{R}$ and that the functionals considered previously in the furtivity and in the masking problems in [1], [4] seem to be "local" in the previous sense. Hence, one of the difficulties of the model (10), (1), (4)–(6) is the "non-local" character of the functional given in (9). Note that the terminology "local" has been used previously in a slightly different sense. We reconsider more accurately the issue of "locality" later on.

We overcome this difficulty by making the following assumptions: let $(r,\theta,\phi)$ be the usual spherical polar coordinate system in $\mathbb{R}^3$ with center in the origin, let $B = B_1$ be a sphere with center in the origin and unit radius, and let $\partial B$ be its boundary; we assume that:

(a) The boundary of the obstacle $\Omega$ is a star-like surface with respect to the origin, that is, $\Omega$ and $\partial\Omega$ can be represented as follows:

$$\Omega = \{\underline{x} = r\hat{\underline{x}} \in \mathbb{R}^3 \mid 0 \le r < \xi(\hat{\underline{x}}), \hat{\underline{x}} \in \partial B\}, \tag{11}$$

$$\partial\Omega = \{\underline{x} = r\hat{\underline{x}} \in \mathbb{R}^3 \mid r = \xi(\hat{\underline{x}}), \hat{\underline{x}} \in \partial B\}, \tag{12}$$

where $\xi(\hat{\underline{x}}) > 0$, $\hat{\underline{x}} \in \partial B$, is a single-valued function defined on $\partial B$ that is assumed sufficiently regular for the manipulations that follow.

(b) The sets $\Omega_\epsilon$ and $\partial\Omega_\epsilon$ can be represented as follows:

$$\Omega_\epsilon = \{\underline{x} = r\hat{\underline{x}} \in \mathbb{R}^3 | 0 \le r < (\xi(\hat{\underline{x}}) + \epsilon), \hat{\underline{x}} \in \partial B\}, \quad \epsilon > 0, \tag{13}$$

$$\partial\Omega_\epsilon = \{\underline{x} = r\hat{\underline{x}} \in \mathbb{R}^3 \mid r = \xi(\hat{\underline{x}}) + \epsilon, \hat{\underline{x}} \in \partial B\}, \quad \epsilon > 0. \tag{14}$$

Assumptions (a) and (b) are only two of many other possible choices made to guarantee the satisfactory solution of the model (10), (1), (4)–(6). This choice is made just to fix ideas and to keep the exposition simple.

Under assumptions (a) and (b), applying the Pontryagin maximum principle, we find that the optimal state trajectory $\tilde{u}^s$, and the corresponding adjoint-variable trajectory $\tilde{\varphi}$ satisfy the necessary first-order optimality conditions associated to the optimal-control problem (1), (4)–(6), (10). That is, they are the solutions of the following exterior problem for a system of two coupled wave equations:

$$\triangle\tilde{u}^s(\underline{x},t) - \frac{1}{c^2}\frac{\partial^2\tilde{u}^s}{\partial t^2}(\underline{x},t) = 0, \quad (\underline{x},t) \in (\mathbb{R}^3 \setminus \overline{\Omega}) \times \mathbb{R}, \tag{15}$$

$$\tilde{u}^s(\underline{x},t) = O\left(\frac{1}{r}\right), \quad r \to +\infty,\ t \in \mathbb{R}, \tag{16}$$

$$\frac{\partial\tilde{u}^s}{\partial r}(\underline{x},t) + \frac{1}{c}\frac{\partial\tilde{u}^s}{\partial t}(\underline{x},t) = o\left(\frac{1}{r}\right), \quad r \to +\infty,\ t \in \mathbb{R}, \tag{17}$$

$$-\frac{\partial\tilde{u}^s}{\partial t}(\underline{x},t) + c\chi\frac{\partial\tilde{u}^s}{\partial\underline{n}(\underline{x})}(\underline{x}) = g(\underline{x},t) - \frac{(1+\chi)}{2\mu\varsigma}\tilde{\varphi}(\underline{x},t), \quad (\underline{x},t) \in \partial\Omega \times \mathbb{R}, \tag{18}$$

$$\triangle\tilde{\varphi}(\underline{x},t) - \frac{1}{c^2}\frac{\partial^2\tilde{\varphi}}{\partial t^2}(\underline{x},t) = 0, \quad (\underline{x},t) \in (\mathbb{R}^3 \setminus \overline{\Omega}) \times \mathbb{R}, \tag{19}$$

$$\tilde{\varphi}(\underline{x},t) = O\left(\frac{1}{r}\right), \quad r \to +\infty,\ t \in \mathbb{R}, \tag{20}$$

$$\frac{\partial\tilde{\varphi}}{\partial r}(\underline{x},t)-\frac{1}{c}\frac{\partial\tilde{\varphi}}{\partial t}(\underline{x},t)=o\left(\frac{1}{r}\right),\quad r\to+\infty,\ t\in\mathbb{R}, \tag{21}$$

$$-\frac{\partial\tilde{\varphi}}{\partial t}(\underline{x},t)-c\chi\frac{\partial\tilde{\varphi}}{\partial\underline{n}(\underline{x})}(\underline{x})=-2\lambda(1+\chi)f_\epsilon\left(\frac{\underline{x}}{\|\underline{x}\|}\right)\times\int_{\mathbb{R}}\mathrm{d}\tau\ \check{I}_k(\tau)\left(\tilde{u}^s\left(\underline{x}+\epsilon\frac{\underline{x}}{\|\underline{x}\|},t-\tau\right)\right.$$
$$\left.-u^s_G\left(\underline{x}+\epsilon\frac{\underline{x}}{\|\underline{x}\|},t-\tau\right)\right),\ (\underline{x},t)\in\partial\Omega\times\mathbb{R}, \tag{22}$$

$$\lim_{t\to-\infty}\tilde{u}^s(\underline{x},t)=0,\quad \underline{x}\in\mathbb{R}^3\setminus\overline{\Omega}, \tag{23}$$

$$\lim_{t\to+\infty}\tilde{\varphi}(\underline{x},t)=0,\quad \underline{x}\in\mathbb{R}^3\setminus\Omega, \tag{24}$$

where $f_\epsilon(\underline{x}/\|\underline{x}\|)$, $\underline{x}\in\partial\Omega$ is the function defined by

$$f_\epsilon\left(\frac{\underline{x}}{\|\underline{x}\|}\right)=f_\epsilon(\hat{\underline{x}}(\theta,\phi))=\frac{v_\epsilon(\theta,\phi)}{v(\theta,\phi)},\quad \underline{x}\in\partial\Omega,\quad \hat{\underline{x}}=\frac{\underline{x}}{\|\underline{x}\|}\in\partial B,\ 0\le\theta\le\pi,\ 0\le\phi<2\pi, \tag{25}$$

with

$$v(\theta,\phi)=\xi\sqrt{\left(\frac{\partial\xi}{\partial\theta}\right)^2\sin^2\theta+\left(\frac{\partial\xi}{\partial\phi}\right)^2+\xi^2\sin^2\theta},\quad 0\le\theta\le\pi,\ 0\le\phi<2\pi, \tag{26}$$

$$v_\epsilon(\theta,\phi)=(\xi+\epsilon)\sqrt{\left(\frac{\partial\xi}{\partial\theta}\right)^2\sin^2\theta+\left(\frac{\partial\xi}{\partial\phi}\right)^2+(\xi+\epsilon)^2\sin^2\theta},\quad 0\le\theta\le\pi,\ 0\le\phi<2\pi. \tag{27}$$

The relation between $\tilde{\varphi}$ and the optimal-control solution of problem (1), (4–6), (10), $\tilde{\psi}$ is

$$\tilde{\psi}(\underline{x},t)=-\frac{1}{2\mu\varsigma}\tilde{\varphi}(\underline{x},t),\quad (\underline{x},t)\in\partial\Omega\times\mathbb{R}. \tag{28}$$

For future convenience, we point out that

$$\mathrm{d}s_{\partial\Omega}=v(\theta,\phi)\mathrm{d}\theta\,\mathrm{d}\phi,\quad 0\le\theta\le\pi,\ 0\le\phi<2\pi, \tag{29}$$

and

$$\mathrm{d}s_{\partial\Omega_\epsilon}=v_\epsilon(\theta,\phi)\mathrm{d}\theta\,\mathrm{d}\phi,\quad 0\le\theta\le\pi,\ 0\le\phi<2\pi. \tag{30}$$

In order to guarantee conditions (23) and (24), we must choose the incident wave in a suitable class of functions, as will be done in Section 2. Furthermore, the boundary conditions (18) and (22) can be slightly adapted to deal with the limiting case $\chi=+\infty$. Finally, we emphasize that using the terminology introduced before, the boundary condition (22) given on $\partial\Omega$ has a "non-local" character since it depends on the values of the function $\tilde{u}^s$ on the surface $\partial\Omega_\epsilon$. Moreover, condition (22) at time $t$ depends on the values of $\tilde{u}^s(\underline{x},\tau)$ with $\tau\in\mathbb{R}$. Indeed, the dependence of the boundary conditions (18), (22) on the values of $\tilde{u}^s$ for $\underline{x}\notin\partial\Omega$ is also contained in the normal derivative $\partial\cdot/\partial\underline{n}$ that appears in (18) and (22). That "non-locality" of the boundary conditions (18) and (22) is not a specific characteristic of the definite-band ghost-obstacle problem, and it was already present through the term involving the normal derivative in the furtivity and masking problems considered in [1, 4] while the "non-locality" of the functional $F_{\lambda,\mu,\epsilon}$ given in (9) is a specific characteristic of the definite-band ghost problem and also the dependence of (22) at time $t$ on the values $\tilde{u}^s(\underline{x},\tau)$ with $\tau\in\mathbb{R}$ seems to be a specific non-local characteristic of definite-band problems. That is, the "non-locality" appears in the definite-band problems in a new form. Later, we will see that the assumptions made make it possible to reduce the solution of (15)–(24) to the solution of a family of boundary-value problems for two coupled Helmholtz equations depending on a real parameter.

The definite-band furtivity problem can be modelled as the control problem (1), (4)–(6), (10) when we replace $\Omega_\epsilon$ with $\Omega$, $u_G^s$ with zero (that is when $\Omega_G = \emptyset$), and, as a consequence, $f_\epsilon$ with one. Furthermore, the necessary first-order optimality conditions associated with the optimal control problem (1), (4–6), (10) associated with the definite-band furtivity problem are given by the zero-order term in $\epsilon$ for $\epsilon \to 0^+$ in Eqs. (15)–(24), replacing $u_G^s$ with zero in Eq. (22).

The furtivity problem and the ghost-obstacle problem studied in [1–5] can be considered as particular cases of the corresponding definite-band problems. The furtivity problem, studied in [1] can be interpreted as an "infinite" band furtivity problem; in fact, the furtivity problem of [1] amounts to making the wave scattered by the obstacle as small as possible in the entire frequency space (i.e., corresponds to the choice $K = \mathbb{R}$). In [1], a mathematical formulation of the furtivity problem as a control problem is given, and the functional cost proposed is, roughly speaking, a particular case of the cost functional (9) when we choose $K = \mathbb{R}$, $\Omega_G = \emptyset$, $f_\epsilon(\underline{x}/\|\underline{x}\|) = 1$, $\underline{x}/\|\underline{x}\| \in \partial B$ and we replace $\Omega_\epsilon$ with $\Omega$ and $u_G^s$ with zero.

Recall that when we pass from an "infinite" band to a "definite" band, the cost functional and, as a consequence, the corresponding first-order optimality conditions, change substantially. One could ask the reason for restricting the furtivity effect on a definite-band $K$ when the smart obstacle can be made furtive on the entire band (i.e., $K = \mathbb{R}$) of the frequency space. The answer lies in the fact that we expect that achieving the goal of the furtivity problem (i.e., the choice $K = \mathbb{R}$) should be more "expensive" in terms of the control function employed than achieving the same goal in the definite-band problem (i.e.: the choice $K \subset \mathbb{R}$). A norm of the optimal-control function $\psi$ will be used to measure how expensive it is to achieve a given goal. The same can be said for the ghost-obstacle problem. We will show in Section 4 for some test problems that, when we solve the furtivity problem or the ghost-obstacle problem, we "spend" more in terms of the control function $\psi$ acting on the boundary of the obstacle than when we solve the definite-band furtivity problem or the definite-band ghost-obstacle problem, respectively. Furthermore, we will show that the "size" of the control function employed to pursue the goal proposed on the set $K$ "increases" when the "size" of the set $K$ increases. We should also mention that definite-band problems are more realistic; in fact, in many applications smart objects pursue their goals only on a definite band in the frequency space; for examples see [6–9].

The mathematical formulation of the definite-band ghost-obstacle problem as the optimal control problem (1), (4–6), (10) and the successive reduction under the hypotheses (a) and (b) of problem (1), (4–6), (10) to the solution of the exterior problem (15)–(24) provide us with a practical tool for solving the definite-band ghost-obstacle problem. A similar statement holds for the definite-band furtivity problem.

### 1.2 A brief discussion on the numerical solution of the optimal-control problem for the definite-band ghost-obstacle problem

The most common numerical methods for solving a control problem such as (1), (4)–(6), (10) involve the iterative solution of the scattering problem (1), (4)–(6). These approaches are time-consuming and not always practical in real situations. We avoid this iterative approach thanks to the use of the Pontryagin maximum principle (see [13, Chapter 9], [14, Chapter 3], [15, Chapter 6] for a survey of optimal-control problems for partial differential equations). In fact, thanks to the assumptions made when applying the Pontryagin maximum principle, we can formulate the first-order optimality conditions for the definite-band ghost-obstacle problem as the exterior problem (15)–(24) for two coupled wave equations, that is, we can solve the optimal-control problem (1), (4)–(6), (10) approximately at the computational cost needed to solve the exterior problem (1), (2), (4), (5). This is a relevant advantage in many practical situations, as emphasized also in [1–4]. The exterior problem (15)–(24) can be solved with several well-known methods used for the numerical solution of partial differential equations, such as, finite-difference or finite-element methods, integral-equation methods, and so on. However, since the solution of systems of coupled partial differential equations such as (15)–(24) is computationally expensive, the use of a solver with high parallel

performance is desirable. For this purpose, we have developed a numerical method based on the so-called "operator expansion method" as proposed in [1, 11]. The "operator-expansion method" was introduced by Milder [16] and, in its many versions, has been widely used to solve problems in acoustics and electromagnetics (see for example [1–5, 11], [16]–[24]). In this paper, we reformulate the "operator-expansion method" in order to provide a highly parallelizable method to solve the exterior problem (15)–(24) for $\epsilon > 0$, that is, to solve the definite-band ghost-obstacle problem and to solve the definite-band furtivity problem that is to solve the exterior problem (15)–(24) when $\epsilon = 0, f_\epsilon = 1$ and when we replace $u_G^s$ with zero in Eq. 22.

We note that the optimal-control problems formulated in this paper are solved as open-loop control problems due to the condition imposed when $t \to +\infty$. It is known that their solution through the equations that correspond to the first-order optimality conditions is not a robust approach to the control problem. Indeed, the mathematical formulation of the furtivity problem as a closed-loop control problem can be studied, and an infinite-dimensional Riccati equation that solves the problem can be derived. The solution of this equation appears more expensive computationally than the solution of the exterior problem (15)–(24), since, to the best of our knowledge, there are no ad hoc solvers for these Riccati equations. However, the main reason to justify the use of the open-loop formulation is that, in the practical situations that we have in mind where the mathematical model proposed here can be used, the incoming signal to consider is a sequence of identical acoustic impulses. The problem of making an obstacle smart when hit by a sequence of acoustic impulses is a problem substantially made up of many independent identical problems, that is, one problem for each impulse, wherein the obstacle does not interact with an impulse before and after the impact of that impulse on the obstacle. So that, in this case, the control function that must act on the boundary of the obstacle can be computed when the obstacle is hit by the first impulse and then repeated when the successive impulses reach the obstacle, that is, the obstacle is made smart with respect to the impact of the first impulse and its behavior remains "smart" in the future repeating the optimal pressure current computed due to the special form of the incoming acoustic field. The absence of smart behavior when the first impulse interacts with the obstacle may be tolerated since, due to the presence of noise, only repeated detection is considered reliable in most detection devices. Furthermore, the open-loop approach leads to the first-order optimality conditions (15)–(24) that can be efficiently solved via the modified version of the operator-expansion method proposed in Section 3 that gives useful results when used in some test cases.

An intermediate approach that could be used here between the open- and closed-loop approach is the receding-horizon control of linear infinite-dimensional systems (see for example [25–27]). This approach approximates the optimal infinite-horizon control with a finite-horizon suboptimal control, where the horizon goes from the current time to the current time plus a fixed horizon length and, in the most naive implementation, the state variable is constrained at the final time. The receding-horizon implementation is typically formulated by introducing an open-loop optimization problem. Several formulations of the receding time horizon have been studied in order to guarantee stability and to avoid equality constraints on the state variable at the final time since the treatment of this last type of constraints is computationally demanding (see [25–27]).

We are not pursuing this approach for two reasons. First, as discussed previously, the particular features of the control problems considered (i.e., the incoming signal composed of a sequence of identical impulses) make satisfactory the use of the open-loop approach to determine the optimal solution. Second, as emphasized in [25], the receding-horizon control of nonlinear systems is an efficient approach when we can solve sequentially open-loop fixed-horizon optimal-control problems at low computational cost, and this does not apply to our case. In fact, even using the order-reduction method to approximate the partial differential equations with finite-dimensional dynamical systems (see, for example, [28, 29]) to solve the sequence of open-loop finite-horizon problems coming from the receding-horizon approach, we have that the computational effort required to solve the optimal control problem (1), (4)–(6), (10) using the finite horizon method will be prohibitive compared to the computational effort required by the method suggested in this paper. Moreover, only a suboptimal solution is obtained using the finite-horizon method.

In fact, due to the particular incoming signal and to the assumptions made on the scatterer, the solution method suggested in this paper can reduce the solution of the optimal control problem (1), (4–6), (10) to the solution of a few hundreds diagonal systems of linear equations in a few hundreds unknowns. In fact, we reduce the control problem via the use of the Pontryagin maximum principle and some other suitable assumptions to a system of partial differential equations for the state variable $u^s$ and the adjoint variable $\varphi$. This system of partial differential equations, owing to its particular form, is very well suited to be solved with the so-called "operator-expansion method" (see [1, 4, 11]). The "operator-expansion method" under suitable assumption on $u^i$ allows us to represent $u^i$ itself, the state variable (i.e., the scattered field) and the adjoint variable (see formulae (51–53)) as a superposition of 30–40 really significant time-harmonic waves. Hence, thanks to the formulae (51–54), we reduce the time-dependent equations (15)–(22) to a set of Helmholtz equations with suitable boundary conditions, that is, Eqs. (55)–(58) and then via assumptions $(e_2)$ and formulae (64), (65), (94), (95) we reduce the solution of Eqs. (55)–(58) to the solution of the integral equations (83), (84) defined on the boundary of the sphere $B_1$ that can be solved with very small computational effort owing to the use of the operator-expansion method. Roughly speaking, using the spherical-harmonics basis to solve the boundary-value problems we can reduce the computation to the solution of 30–150 diagonal linear systems involving about 300 unknowns, each dependent on the order of the expansion used in the "operator-expansion method". Hence, the use of some other order-reduction techniques, such as those proposed in [28, 29] is not justified. The operator-expansion method in the form presented here is an ad hoc solver that cannot solve the generic scattering problem. In conclusion, the use of the receding-horizon approach to control problems and of the order-reduction method to approximate partial differential equations is not justified when we consider simple scattering problems like the ones considered here, although it may be justified or even necessary if more difficult problems are considered.

The main restriction of the approach proposed in this paper is that the shape of the obstacles must be not far from spherical. This limitation is intrinsic with the operator-expansion proposed in [1, 11], since the time-dependent scattering problem is reduced to a set of integral equations defined on a sphere. Only recently in the study of the standard scattering problems this limitation has been overcome by new versions of the operator-expansion method [30]. However, the extension of the expansion discussed in [30] to optimal-control problems is beyond the scope of this paper.

In the following, we focus our attention on the solution of the definite-band ghost-obstacle problem and, where necessary, underline how the analysis must be modified to deal with the definite-band furtivity problem.

### 1.3 Outline of the paper

In Section 2, we derive the first-order optimality conditions of the control problem (1), (4)–(6), (10) that is, Eqs. (15)–(24). In Section 3, we give a brief description of the modified versions of "operator-expansion" method needed to solve the exterior problem (15)–(24), and point out the differences with the versions of the "operator-expansion method" proposed in [1, 4, 11]. In Section 4, we validate the mathematical model and the numerical methods proposed for solving some test problems. Impressive speed-up factors are obtained by running a parallel implementation of the numerical methods developed. Some animations and virtual-reality applications relative to the numerical experiments proposed in Section 4 can be found in the website: `http://www.econ.univpm.it/recchioni/w11`. In Section 5 several conclusions will be drawn.

## 2 The first-order optimality conditions for the definite-band ghost-obstacle problem

We study the optimal-control problem (1), (4)–(6), (10). For simplicity, we consider only the case $0 < \mu < 1$. Remember that the cases $\mu = 0, 1$ are trivial, as shown in [1]. In order to apply the Pontryagin maximum

principle to (1), (4)–(6), (10) we reduce the integral on $\partial\Omega_\epsilon$ to an integral on $\partial\Omega$ using assumptions (a) and (b) of Section 1. In fact, from assumptions (a) and (b) and formulae (25), (29), (30), we have:

$$\mathrm{d}s_{\partial\Omega_\epsilon}\left(\underline{x}+\epsilon\frac{\underline{x}}{\|\underline{x}\|}\right)=f_\epsilon\left(\frac{\underline{x}}{\|\underline{x}\|}\right)\mathrm{d}s_{\partial\Omega}(\underline{x}),\quad \underline{x}\in\partial\Omega, \tag{31}$$

and the cost functional (9) can be rewritten as:

$$F_{\lambda,\mu,\epsilon}(\psi)=\int_{\mathbb{R}}\mathrm{d}t\int_{\partial\Omega}(1+\chi)\left\{\lambda\, C^2_{K,u^s,u^s_G}\left(\underline{x}+\epsilon\frac{\underline{x}}{\|\underline{x}\|},t\right)f_\epsilon\left(\frac{\underline{x}}{\|\underline{x}\|}\right)+\mu\varsigma\psi^2(\underline{x},t)\right\}\mathrm{d}s_{\partial\Omega}(\underline{x}). \tag{32}$$

Because of Eq. (32), we can proceed to the application of the Pontryagin maximum principle as in [1, Section 2].

Let us introduce the vector space C of admissible controls and some other useful function spaces. Let us denote by $u^s|_{\partial\Omega}$, $\varphi|_{\partial\Omega}$, $u^s|_{\partial\Omega_\epsilon}$ and $\varphi|_{\partial\Omega_\epsilon}$ the restrictions of $u^s$ and $\varphi$ to $\partial\Omega$ and to $\partial\Omega_\epsilon$, respectively, and let $L^\infty(\partial\Omega)$ be the space of real functions defined on $\partial\Omega$ essentially bounded on $\partial\Omega$ (with respect to $\mathrm{d}s_{\partial\Omega}$); similarly, we can define $L^\infty(\partial\Omega_\epsilon)$, $\epsilon>0$. Let $L^2(\partial\Omega\times\mathbb{R})$ be the usual space of real functions defined on $\partial\Omega\times\mathbb{R}$, square integrable with respect to the measures $\mathrm{d}s_{\partial\Omega}\mathrm{d}t$. Similarly, we can define $L^2(\partial\Omega_\epsilon\times\mathbb{R})$, $\epsilon>0$. We define the following spaces of functions:

$$\mathcal{C}=\left\{\mathcal{F}:(\mathbb{R}^3\setminus\Omega)\times\mathbb{R}\to\mathbb{R}\text{ such that }:\mathcal{F}|_{\partial\Omega\times\mathbb{R}},\ \frac{\partial\mathcal{F}}{\partial\underline{n}}|_{\partial\Omega\times\mathbb{R}},\ \frac{\partial\mathcal{F}}{\partial t}|_{\partial\Omega\times\mathbb{R}}\in L^2(\partial\Omega\times\mathbb{R}),\right.$$

$\mathcal{F}$ satisfies equations (1), (4) and the following condition at infinity:

$$\left.\frac{\partial\mathcal{F}}{\partial r}(\underline{x},t)-\frac{1}{c}\frac{\partial\mathcal{F}}{\partial t}(\underline{x},t)=o\left(\frac{1}{r}\right),\quad r\to+\infty,\quad t\in\mathbb{R}\right\}, \tag{33}$$

$$\mathcal{U}=\left\{\mathcal{F}:(\mathbb{R}^3\setminus\Omega)\times\mathbb{R}\to\mathbb{R}\text{ such that }:\mathcal{F}|_{\partial\Omega\times\mathbb{R}},\ \frac{\partial\mathcal{F}}{\partial\underline{n}}|_{\partial\Omega\times\mathbb{R}},\ \frac{\partial\mathcal{F}}{\partial t}|_{\partial\Omega\times\mathbb{R}}\in L^2(\partial\Omega\times\mathbb{R})\right.,$$

$\mathcal{F}|_{\partial\Omega_\epsilon\times\mathbb{R}}\in L^2(\partial\Omega_\epsilon\times\mathbb{R})$, $\epsilon>0$, $\mathcal{F}$ satisfies Eqs. (1), (4) and the following condition at infinity:

$$\left.\frac{\partial\mathcal{F}}{\partial r}(\underline{x},t)+\frac{1}{c}\frac{\partial\mathcal{F}}{\partial t}(\underline{x},t)=o\left(\frac{1}{r}\right),\quad r\to+\infty,\quad t\in\mathbb{R}\right\}, \tag{34}$$

and

$$\mathrm{C}=\left\{f\in L^2(\partial\Omega\times\mathbb{R}),\ f(\underline{x},t)\in L^\infty(\partial\Omega),\ t\in\mathbb{R},\text{ moreover there exists}\right.$$
$$\left.F\in\mathcal{C}\text{ such that }F|_{\partial\Omega\times\mathbb{R}}=f\text{ and }\lim_{t\to+\infty}F(\underline{x},t)=0,\ \underline{x}\in\mathbb{R}^3\setminus\overline{\Omega}\right\}, \tag{35}$$

$$\mathrm{U}=\left\{f\in L^2(\partial\Omega\times\mathbb{R}),\ f(\underline{x},t)\in L^\infty(\partial\Omega),\ t\in\mathbb{R},\text{ moreover there exists}\right.$$
$$\left.F\in\mathcal{U}\text{ such that }F|_{\partial\Omega\times\mathbb{R}}=f\text{ and }\lim_{t\to-\infty}F(\underline{x},t)=0,\ \underline{x}\in\mathbb{R}^3\setminus\overline{\Omega}\right\}. \tag{36}$$

Note that the set C defined in (35) is the space of admissible controls. From (32) it follows that the optimal control problem (1), (4)–(6), (10) can be associated with the following Hamiltonian (see [13, p. 35], [31, p. 19]):

$$\begin{aligned}H(u^s,\psi,\varphi,t)=&-(1+\chi)\int_{\partial\Omega}\mathrm{d}s_{\partial\Omega}(\underline{x})\left\{\lambda f_\epsilon\left(\frac{\underline{x}}{\|\underline{x}\|}\right)C^2_{K,u^s,u^s_G}\left(\underline{x}+\epsilon\frac{\underline{x}}{\|\underline{x}\|},t\right)+\mu\varsigma\psi^2(\underline{x},t)\right\}\\&+\int_{\partial\Omega}\mathrm{d}s_{\partial\Omega}(\underline{x})\left\{\varphi(\underline{x},t)\left[c\chi\frac{\partial u^s}{\partial\underline{n}}(\underline{x},t)-(1+\chi)\psi(\underline{x},t)-g(\underline{x},t)\right]\right\},\quad u^s\in\mathrm{U},\quad\varphi\in\mathrm{C},\quad t\in\mathbb{R}.\end{aligned} \tag{37}$$

In the Hamiltonian (37), the second adjoint variable, that is, the one that should appear inside the first integral in (37), has been set to $-1$. This is a legitimate choice as explained in [1, Section 2]. Furthermore, the Hamiltonian (37) can deal with the limit case $\chi = +\infty$ with minor modifications.

The functional derivatives $\delta H/\delta\varphi$, $\delta H/\delta u^s$, are defined by the following equations:

$$H(u^s, \psi, \varphi + \delta\varphi, \varphi_0, t) - H(u^s, \psi, \varphi, \varphi_0, t) = \int_{\partial\Omega} \mathrm{d}s_{\partial\Omega} \frac{\delta H}{\delta\varphi}\delta\varphi + \epsilon_1(\delta\varphi), \quad \delta\varphi \in \mathrm{C},\ t \in \mathbb{R}, \tag{38}$$

$$H(u^s + \delta u^s, \psi, \varphi, \varphi_0, t) - H(u^s, \psi, \varphi, \varphi_0, t) = \int_{\partial\Omega} \mathrm{d}s_{\partial\Omega} \frac{\delta H}{\delta u^s}\delta u^s + \epsilon_2(\delta u^s), \quad \delta u^s \in \mathrm{U},\ t \in \mathbb{R}, \tag{39}$$

where $\epsilon_1(\delta\varphi) = o(\delta\varphi)$ when $\delta\varphi$ goes to zero and $\epsilon_2(\delta u^s) = o(\delta u^s)$ when $\delta u^s$ goes to zero. Note that $\delta H/\delta\varphi$ must be independent of $\delta\varphi$ and that $\delta H/\delta u^s$ must be independent of $\delta u^s$.

We note that, when for $\underline{x} \in \partial\Omega$, the incoming wave packet goes to zero when $t \to -\infty$ we have that, for any $\psi \in \mathrm{C}$, the corresponding scattered wave $u^s(\underline{x}, t)$ solution of problem (1), (4)–(6) satisfies the condition $\lim_{t\to-\infty} u^s(\underline{x}, t) = 0$, $\underline{x} \in \mathbb{R}^3 \setminus \overline{\Omega}$. Applying the Pontryagin maximum principle to the Hamiltonian given in (37) (see [13, Theorem 1, p. 36] or [31, Theorem 1, p. 20], [1, p. 559]) we find that the following conditions must be satisfied by the optimal control $\tilde{\psi}$, the corresponding optimal state trajectory $\tilde{u}^s$ and the corresponding adjoint variable $\tilde{\varphi}$:

$$\frac{\partial\tilde{u}^s}{\partial t}(\underline{x}, t) = \left(\frac{\delta H}{\delta\varphi}\right)(\tilde{u}^s, \tilde{\psi}, \tilde{\varphi}, \underline{x}, t), \quad (\underline{x}, t) \in \partial\Omega \times \mathbb{R}, \tag{40}$$

$$\frac{\partial\tilde{\varphi}}{\partial t}(\underline{x}, t) = -\left(\frac{\delta H}{\delta u^s}\right)(\tilde{u}^s, \tilde{\psi}, \tilde{\varphi}, \underline{x}, t), \quad (\underline{x}, t) \in \partial\Omega \times \mathbb{R}, \tag{41}$$

$$H(\tilde{u}^s, \tilde{\psi}, \tilde{\varphi}, t) \geq H(\tilde{u}^s, \psi, \tilde{\varphi}, t), \quad \psi \in \mathrm{C},\ t \in \mathbb{R}, \tag{42}$$

together with the following "transversality condition":

$$\lim_{t\to+\infty} \tilde{\varphi}(\underline{x}, t) = 0, \quad \underline{x} \in \partial\Omega. \tag{43}$$

In the remainder of this section, we extend the notation, in fact when $v \in \mathrm{C}$ or $v \in \mathrm{U}$, we continue to denote with $v$ the function $F$ belonging, respectively, to $\mathcal{C}$ or $\mathcal{U}$, such that $F|_{\partial\Omega\times\mathbb{R}} = v$.

Now, we show that the first-order optimality conditions associated with the control problem (1), (4–6), (10) with $0 < \mu < 1$ are given by (15)–(24). Note that the adjoint variable $\tilde{\varphi}$ is chosen as a function defined on $(\mathbb{R}^3 \setminus \overline{\Omega}) \times \mathbb{R}$ satisfying some equations (i.e., (19)–(21)) and that the trace of $\tilde{\varphi}$ on $\partial\Omega \times \mathbb{R}$ is still denoted by $\tilde{\varphi}$.

We start by showing the relation between the optimal control $\tilde{\psi}$ of problem (1), (4)–(6), (10) and the adjoint variable $\tilde{\varphi}$. We have

$$H(\tilde{u}^s, \tilde{\psi}, \tilde{\varphi}, t) = \max_{\psi\in\mathrm{C}} H(\tilde{u}^s, \psi, \tilde{\varphi}, t), \quad t \in \mathbb{R}, \tag{44}$$

that is,

$$\begin{aligned} H(\tilde{u}^s, \tilde{\psi}, \tilde{\varphi}, t) = {} & \int_{\partial\Omega} \mathrm{d}s_{\partial\Omega}(\underline{x}) \left\{ -(1+\chi)\lambda f_\epsilon \left(\frac{\underline{x}}{\|\underline{x}\|}\right) C^2_{K,u^s,u^s_G}(\underline{x}, t) + \tilde{\varphi}(\underline{x}, t) \left[ c\chi \frac{\partial\tilde{u}^s}{\partial\underline{n}}(\underline{x}, t) - g(\underline{x}, t) \right] \right\} \\ & + \max_{\psi\in\mathrm{C}} \left\{ \int_{\partial\Omega} \mathrm{d}s_{\partial\Omega}(\underline{x}) \left[ -(1+\chi)\mu\varsigma\psi^2(\underline{x}, t) - \tilde{\varphi}(\underline{x}, t)(1+\chi)\psi(\underline{x}, t) \right] \right\}, \quad t \in \mathbb{R}. \end{aligned} \tag{45}$$

Imposing the necessary first-order optimality condition, i.e., $\frac{\delta H}{\delta\psi}(\tilde{u}^s, \tilde{\psi}, \tilde{\varphi}, t) = 0$, we obtain

$$\int_{\partial\Omega} \mathrm{d}s_{\partial\Omega}(\underline{x}) \left[ -2(1+\chi)\mu\varsigma\tilde{\psi}(\underline{x}, t) - (1+\chi)\tilde{\varphi}(\underline{x}, t) \right] \delta\psi(\underline{x}, t) = 0, \quad \delta\psi \in \mathrm{C}, \quad t \in \mathbb{R}, \tag{46}$$

that is, Eq. (28). Let $\tilde{\varphi} \in \mathrm{C}$ and $\delta\tilde{u}^s \in \mathrm{U}$, as proved in [1, pp. 560–561] we have

$$\int_{\partial\Omega} \mathrm{d}s_{\partial\Omega}(\underline{x}) \left(\tilde{\varphi}\frac{\partial}{\partial \underline{n}}\delta\tilde{u}^s\right)(\underline{x},t) = \int_{\partial\Omega} \mathrm{d}s_{\partial\Omega}(\underline{x}) \left(\delta\tilde{u}^s \frac{\partial\tilde{\varphi}}{\partial \underline{n}}\right)(\underline{x},t), \quad t \in \mathbb{R}. \tag{47}$$

Owing to Eq. (47), we can compute the functional derivatives $\delta H/\delta\varphi$, $\delta H/\delta u^s$ defined in (38), (39), respectively. From (38), since $\delta\tilde{u}^s \in \mathrm{U}$ and $\tilde{\varphi} \in \mathrm{C}$, they have extensions in $(\mathbb{R}^3\backslash\Omega) \times \mathbb{R}$ that satisfy the wave equation and belong to $\mathcal{U}$ and $\mathcal{C}$, respectively; we have

$$\begin{aligned} &H(\tilde{u}^s, \tilde{\psi}, \tilde{\varphi} + \delta\tilde{\varphi}, t) - H(\tilde{u}^s, \tilde{\psi}, \tilde{\varphi}, t) = \\ &\int_{\partial\Omega} \mathrm{d}s_{\partial\Omega}(\underline{x})\delta\tilde{\varphi}(\underline{x},t)\left(c\chi\frac{\partial\tilde{u}^s}{\partial \underline{n}}(\underline{x},t) - (1+\chi)\tilde{\psi}(\underline{x},t) - g(\underline{x},t)\right) + \varepsilon_1(\delta\tilde{\varphi}), \quad \delta\tilde{\varphi} \in \mathrm{C}, \quad t \in \mathbb{R}, \end{aligned} \tag{48}$$

where $\varepsilon_1(\delta\tilde{\varphi}) = o(\delta\tilde{\varphi})$, when $\delta\tilde{\varphi}$ goes to zero, that is, imposing (40), (42) we have the boundary condition (18). Furthermore, using Eq. (8) and Plancherel's theorem (see [32, Plancherel's Theorem pp. 153]) we have:

$$\begin{aligned} &H(\tilde{u}^s + \delta\tilde{u}^s, \tilde{\psi}, \tilde{\varphi}, t) - H(\tilde{u}^s, \tilde{\psi}, \tilde{\varphi}, t) = \int_{\partial\Omega} \mathrm{d}s_{\partial\Omega}(\underline{x}) \cdot \\ &\left(-2(1+\chi)f_\epsilon\left(\frac{\underline{x}}{\|\underline{x}\|}\right)\lambda\int_{\mathbb{R}} \mathrm{d}s\ \check{I}_K(s)\left(\tilde{u}^s\left(\underline{x}+\epsilon\frac{\underline{x}}{\|\underline{x}\|}, t-s\right) - u^s_G\left(\underline{x}+\epsilon\frac{\underline{x}}{\|\underline{x}\|}, t-s\right)\right)\delta\tilde{u}^s(\underline{x},t)\right. \\ &\left. + \tilde{\varphi}(\underline{x},t)c\chi\frac{\partial}{\partial \underline{n}}(\delta\tilde{u}^s)(\underline{x},t)\right) + \epsilon_2(\delta\tilde{u}^s), \quad \delta\tilde{u}^s \in \mathrm{U}, \quad t \in \mathbb{R}, \end{aligned} \tag{49}$$

where $\epsilon_2(\delta\tilde{u}^s) = o(\delta\tilde{u}^s)$ when $\delta\tilde{u}^s$ goes to zero. Using Eqs. (39) and (47), from (49) we obtain

$$\begin{aligned} \frac{\delta H}{\delta u^s}(\tilde{u}^s, \tilde{\psi}, \tilde{\varphi}, t) = &-2(1+\chi)f_\epsilon\left(\frac{\underline{x}}{\|\underline{x}\|}\right)\lambda\left(\int_{\mathbb{R}} \mathrm{d}s\ \check{I}_K(s)\left(\tilde{u}^s\left(\underline{x}+\epsilon\frac{\underline{x}}{\|\underline{x}\|}, t-s\right) - u^s_G\left(\underline{x}+\epsilon\frac{\underline{x}}{\|\underline{x}\|}, t-s\right)\right)\right) \\ &+ c\chi\frac{\partial\tilde{\varphi}}{\partial \underline{n}}(\underline{x},t), \quad (\underline{x},t) \in \partial\Omega \times \mathbb{R}, \end{aligned} \tag{50}$$

that is, imposing (41) we have the boundary condition (22).

## 3 The operator-expansion method for the definite-band ghost-obstacle problem

The operator-expansion method in the version used here is based on three assumptions that we call $(e_1)$, $(e_2)$, $(e_3)$. Note that the assumptions $(e_1)$, $(e_2)$, $(e_3)$ that we adopt are only one set among many other possible choices that make possible the development of the operator-expansion method.

The first assumption, $(e_1)$, is necessary to reduce the solution of the exterior problem for two coupled wave Eqs. (15)–(24) to the solution of a set of exterior problems for two coupled Helmholtz equations depending on one parameter.

That is, $(e_1)$ assumes that the incident wave $u^i$, the wave $\tilde{u}^s$ scattered by the obstacle $(\Omega;\chi)$, and the adjoint variable $\tilde{\varphi}$ solutions of the exterior problem (15)–(24) can be approximated by a superposition of time-harmonic waves,

$$u^i(\underline{x},t) \approx \sum_{i=1}^{N_1}\sum_{j=1}^{N_2}\left[a_{i,j}\mathrm{e}^{-\mathrm{i}\omega_i t}\mathrm{e}^{\mathrm{i}\omega_i(\underline{x},\underline{\alpha}_j)/c}\right], \quad (\underline{x},t) \in \mathbb{R}^3 \times \mathbb{R}, \tag{51}$$

$$\tilde{u}^s(\underline{x},t) \approx \sum_{i=1}^{N_1}\sum_{j=1}^{N_2}\left[a_{i,j}\mathrm{e}^{-\mathrm{i}\omega_i t}u^s_{\omega_i,\underline{\alpha}_j}(\underline{x})\right], \quad (\underline{x},t) \in (\mathbb{R}^3\backslash\overline{\Omega}) \times \mathbb{R}, \tag{52}$$

$$\tilde{\varphi}(\underline{x},t) \approx \sum_{i=1}^{N_1}\sum_{j=1}^{N_2}\left[a_{i,j}\mathrm{e}^{-\mathrm{i}\omega_i t}\varphi_{\omega_i,\underline{\alpha}_j}(\underline{x})\right], \quad (\underline{x},t) \in (\mathbb{R}^3\backslash\overline{\Omega}) \times \mathbb{R}, \tag{53}$$

where i is the imaginary unit, $N_1, N_2$ are positive integers, $a_{i,j}$, $\omega_i$, $i = 1,2,\ldots,N_1$, $j = 1,2,\ldots,N_2$ are suitable constants and $\underline{\alpha}_j \in \partial B$, $j = 1,2,\ldots,N_2$ are suitable elements of $\partial B$. In Section 4, the choice of $\omega_i$, $a_{i,j}$ and $\underline{\alpha}_j$ will be made depending on the incident wave. In order to formulate the operator-expansion method for the definite-band ghost-obstacle problem, we need the extra assumption that the wave scattered by the ghost-obstacle $(\Omega_G, \chi_G)$ can be also approximated, as done in formula (52),

$$u_G^s(\underline{x},t) \approx \sum_{i=1}^{N_1}\sum_{j=1}^{N_2}\left[a_{i,j}\mathrm{e}^{-\mathrm{i}\omega_i t}u^s_{G,\omega_i,\underline{\alpha}_j}(\underline{x})\right], \quad (\underline{x},t) \in (\mathbb{R}^3\backslash\overline{\Omega_G}) \times \mathbb{R}. \tag{54}$$

Let $W_{N_1,N_2} = \{\omega_1,\omega_2,\ldots,\omega_{N_1}\} \times \{\underline{\alpha}_1,\underline{\alpha}_2,\ldots,\underline{\alpha}_{N_2}\}$. Substituting formulae (51)–(54) in Eqs. (15)–(24), we obtain the following $N_1 \cdot N_2$ exterior problems for a system of two Helmholtz equations; that is, for $(\omega,\underline{\alpha}) \in W_{N_1,N_2}$ we must solve:

$$\left(\triangle u^s_{\omega,\underline{\alpha}} + \frac{\omega^2}{c^2}u^s_{\omega,\underline{\alpha}}\right)(\underline{x}) = 0, \quad \underline{x} \in \mathbb{R}^3\backslash\overline{\Omega}, \tag{55}$$

$$\left(\triangle \varphi_{\omega,\underline{\alpha}} + \frac{\omega^2}{c^2}\varphi_{\omega,\underline{\alpha}}\right)(\underline{x}) = 0, \quad \underline{x} \in \mathbb{R}^3\backslash\overline{\Omega}, \tag{56}$$

$$\mathrm{i}\omega u^s_{\omega,\underline{\alpha}}(\underline{x}) + c\chi\frac{\partial u^s_{\omega,\underline{\alpha}}}{\partial \underline{n}(\underline{x})}(\underline{x}) + \frac{(1+\chi)}{2\mu\varsigma}\varphi_{\omega,\underline{\alpha}}(\underline{x}) = b_{\omega,\underline{\alpha}}(\underline{x}), \quad \underline{x} \in \partial\Omega, \tag{57}$$

$$\mathrm{i}\omega\varphi_{\omega,\underline{\alpha}}(\underline{x}) - c\chi\frac{\partial\varphi_{\omega,\underline{\alpha}}}{\partial\underline{n}(\underline{x})}(\underline{x}) + 2\lambda(1+\chi)f_\epsilon\left(\frac{x}{\|\underline{x}\|}\right)I_k(\omega)\left(u^s_{\omega,\underline{\alpha}}\left(\underline{x}+\epsilon\frac{\underline{x}}{\|\underline{x}\|}\right) - u^s_{G,\omega,\underline{\alpha}}\left(\underline{x}+\epsilon\frac{\underline{x}}{\|\underline{x}\|}\right)\right) = 0, \quad \underline{x}\in\partial\Omega, \tag{58}$$

where $I_K$ is given in formula (7) and $b_{\omega,\underline{\alpha}}$ is given by

$$b_{\omega,\underline{\alpha}}(\underline{x}) = -\mathrm{i}\omega\mathrm{e}^{\mathrm{i}\frac{\omega}{c}(\underline{x},\underline{\alpha})}\left(1+\chi\left(\underline{n}(\underline{x}),\underline{\alpha}\right)\right), \quad \underline{x} \in \partial\Omega, \tag{59}$$

with the following conditions at infinity:

$$\frac{\partial u^s_{\omega,\underline{\alpha}}(\underline{x})}{\partial r} - \mathrm{i}\frac{\omega}{c}u^s_{\omega,\underline{\alpha}}(\underline{x}) = o\left(\frac{1}{r}\right), \quad r \to +\infty, \tag{60}$$

$$\frac{\partial\varphi_{\omega,\underline{\alpha}}(\underline{x})}{\partial r} + \mathrm{i}\frac{\omega}{c}\varphi_{\omega,\underline{\alpha}}(\underline{x}) = o\left(\frac{1}{r}\right), \quad r \to +\infty. \tag{61}$$

We note that $b_{\omega,\underline{\alpha}}(\underline{x})$, $\underline{x} \in \partial\Omega$ is defined almost everywhere in $\underline{x} \in \partial\Omega$, that $u^s_{G,\omega,\underline{\alpha}}$ is defined on $\partial\Omega$ since we have $\partial\Omega \cap \overline{\Omega_G} = \emptyset$, and that formula (58) derives from the following formula:

$$\check{I}_K(t) * \mathrm{e}^{\mathrm{i}zt} = \int_{\mathbb{R}}\mathrm{d}\tau\ \check{I}_K(\tau)\mathrm{e}^{\mathrm{i}z(t-\tau)} = I_K(z)\mathrm{e}^{\mathrm{i}zt}, \quad z \in \mathbb{R}, \ t \in \mathbb{R}, \tag{62}$$

where an asterisk denotes the convolution product. The boundary conditions (57), (58) must be slightly modified when $\chi = +\infty$ (see [1, Section 1]).

We recall that, with a suitable choice of the incident wave packet and space of the admissible control functions, the "initial" condition (23) and the "final" condition (24) will be automatically satisfied.

The second assumption, $(e_2)$, is necessary to solve the exterior problem (55)–(61) with a perturbation method. We note that when the obstacle $\Omega$ and the set $\Omega_\epsilon$ are two concentric spheres, in particular when

$\Omega = B$, that is, when $\xi(\hat{\underline{x}})$ is identically equal to 1 (see (12)), the solution of problem (55)–(61) is given by an explicit series of spherical harmonics (see [33, Eq. (2.48), p. 33]). Let $\Phi_{+\frac{\omega}{c}}$, $\Phi_{-\frac{\omega}{c}}$ be the free-space Green's functions of the Helmholtz operator satisfying the "radiation" conditions (60) and (61), respectively, that is:

$$\Phi_{\pm\frac{\omega}{c}}(\underline{x},\underline{y}) = \frac{\mathrm{e}^{\pm \mathrm{i}\frac{\omega}{c}\|\underline{x}-\underline{y}\|}}{4\pi\|\underline{x}-\underline{y}\|}, \quad \underline{x},\underline{y} \in \mathbb{R}^3, \ \underline{x} \neq \underline{y}. \tag{63}$$

The assumption $(e_2)$ requires:

- $(e_{2,1})$ There exists $a, 0 < a < 1$ such that $\overline{B}_a \subset \Omega$ and the functions $u^s_{\omega,\underline{\alpha}}$ and $\varphi_{\omega,\underline{\alpha}}$, $(\omega,\underline{\alpha}) \in W_{N_1,N_2}$, solutions of problem (55)–(61), can be extended from $\mathbb{R}^3 \setminus \overline{\Omega}$ to $\mathbb{R}^3 \setminus \overline{B}_a$ remaining solutions of the Helmholtz equations (55), (56) in $\mathbb{R}^3 \setminus \overline{B}_a$, respectively;
- $(e_{2,2})$ For $(\omega,\underline{\alpha}) \in W_{N_1,N_2}$, the extensions to $\mathbb{R}^3 \setminus \overline{B}_a$ of $u^s_{\omega,\underline{\alpha}}$, $\varphi_{\omega,\underline{\alpha}}$, that we denote with $U_{\omega,\underline{\alpha}}$, $V_{\omega,\underline{\alpha}}$, respectively, can be represented as single-layer potentials,

$$U_{\omega,\underline{\alpha}}(\underline{x}) = a^2 \int_{\partial B} \Phi_{+\frac{\omega}{c}}(\underline{x}, a\underline{\hat{y}}) \tilde{u}_{\omega,\underline{\alpha}}(\underline{\hat{y}}) \mathrm{d}s_{\partial B}(\underline{\hat{y}}), \quad \underline{x} \in \mathbb{R}^3 \setminus \overline{B}_a, \tag{64}$$

$$V_{\omega,\underline{\alpha}}(\underline{x}) = a^2 \int_{\partial B} \Phi_{-\frac{\omega}{c}}(\underline{x}, a\underline{\hat{y}}) \tilde{v}_{\omega,\underline{\alpha}}(\underline{\hat{y}}) \mathrm{d}s_{\partial B}(\underline{\hat{y}}), \quad \underline{x} \in \mathbb{R}^3 \setminus \overline{B}_a, \tag{65}$$

  for a suitable choice of the density functions $\tilde{u}_{\omega,\underline{\alpha}}(\underline{\hat{y}})$ and $\tilde{v}_{\omega,\underline{\alpha}}(\underline{\hat{y}})$, $\underline{\hat{y}} \in \partial B$;
- $(e_{2,3})$ Assumption (a) of Section 1.1.

It is easy to see that, for any choice of the density functions $\tilde{u}_{\omega,\underline{\alpha}}$, $\tilde{v}_{\omega,\underline{\alpha}}$, that makes formulae (64), (65) differentiable under the integral sign, the functions $U_{\omega,\underline{\alpha}}$, $V_{\omega,\underline{\alpha}}$ satisfy, respectively, the Helmholtz equations (55), (56), and the conditions at infinity (60), (61). Moreover, since $U_{\omega,\underline{\alpha}}$, $V_{\omega,\underline{\alpha}}$ are the extensions of $u^s_{\omega,\underline{\alpha}}$, $\varphi_{\omega,\underline{\alpha}}$, respectively, we determine the density functions $\tilde{u}_{\omega,\underline{\alpha}}$ and $\tilde{v}_{\omega,\underline{\alpha}}$, imposing the boundary conditions (57), (58). That is, for $(\omega, \underline{\alpha}) \in W_{N_1,N_2}$ we obtain the density functions $\tilde{u}_{\omega,\underline{\alpha}}$ and $\tilde{v}_{\omega,\underline{\alpha}}$ as the solutions of the following system of integral equations:

$$\begin{aligned} &\mathrm{i}\omega a^2 \int_{\partial B} \Phi_{+\frac{\omega}{c}}(\underline{x}, a\underline{\hat{y}}) \tilde{u}_{\omega,\underline{\alpha}}(\underline{\hat{y}}) \mathrm{d}s_{\partial B}(\underline{\hat{y}}) + c\chi a^2 \frac{\partial}{\partial \underline{n}(\underline{x})} \int_{\partial B} \Phi_{+\frac{\omega}{c}}(\underline{x}, a\underline{\hat{y}}) \tilde{u}_{\omega,\underline{\alpha}}(\underline{\hat{y}}) \mathrm{d}s_{\partial B}(\underline{\hat{y}}) \\ &\quad + \frac{(1+\chi)}{2\mu\varsigma} a^2 \int_{\partial B} \Phi_{-\frac{\omega}{c}}(\underline{x}, a\underline{\hat{y}}) \tilde{v}_{\omega,\underline{\alpha}}(\underline{\hat{y}}) \mathrm{d}s_{\partial B}(\underline{\hat{y}}) = b_{\omega,\underline{\alpha}}(\underline{x}), \quad \underline{x} = \xi(\hat{\underline{x}})\hat{\underline{x}} \in \partial\Omega, \ \hat{\underline{x}} \in \partial B, \end{aligned} \tag{66}$$

$$\begin{aligned} &\mathrm{i}\omega a^2 \int_{\partial B} \Phi_{-\frac{\omega}{c}}(\underline{x}, a\underline{\hat{y}}) \tilde{v}_{\omega,\underline{\alpha}}(\underline{\hat{y}}) \mathrm{d}s_{\partial B}(\underline{\hat{y}}) - c\chi a^2 \frac{\partial}{\partial \underline{n}(\underline{x})} \int_{\partial B} \Phi_{+\frac{\omega}{c}}(\underline{x}, a\underline{\hat{y}}) \tilde{v}_{\omega,\underline{\alpha}}(\underline{\hat{y}}) \mathrm{d}s_{\partial B}(\underline{\hat{y}}) \\ &\quad + 2\lambda(1+\chi) I_K(\omega) f_\epsilon\left(\frac{\underline{x}}{\|\underline{x}\|}\right) a^2 \int_{\partial B} \Phi_{+\frac{\omega}{c}}(\underline{x} + \epsilon\frac{\underline{x}}{\|\underline{x}\|}, a\underline{\hat{y}}) \tilde{u}_{\omega,\underline{\alpha}}(\underline{\hat{y}}) \mathrm{d}s_{\partial B}(\underline{\hat{y}}) \\ &= 2\lambda(1+\chi) I_K(\omega) f_\epsilon\left(\frac{\underline{x}}{\|\underline{x}\|}\right) u^s_{G,\omega,\underline{\alpha}}\left(\underline{x} + \epsilon\frac{\underline{x}}{\|\underline{x}\|}\right), \quad \underline{x} = \xi(\hat{\underline{x}})\hat{\underline{x}} \in \partial\Omega, \ \hat{\underline{x}} \in \partial B, \end{aligned} \tag{67}$$

where $b_{\omega,\underline{\alpha}}(\underline{x})$, $\underline{x} \in \partial\Omega$ is given by (59). Since $\overline{B}_a \subset \Omega$, the Fredholm integral equations of the first kind (66), (67) have continuous kernels defining compact operators. These equations are ill-posed; as discussed in [1, Section 1], the ill-posedness can be removed by use of a perturbation approach.

Let $(r,\theta,\phi)$ be the canonical spherical polar coordinates of $\underline{x} \in \mathbb{R}^3$; we recall that $r = \|\underline{x}\|$, and write:

$$\hat{\underline{x}}(\theta,\phi) = \frac{\underline{x}}{r} = (\sin\theta\cos\phi, \sin\theta\sin\phi, \cos\theta)^{\mathrm{T}}, \quad 0 \leq \theta \leq \pi, \quad 0 \leq \phi < 2\pi, \tag{68}$$

$$\underline{\hat{x}}_{\theta}(\theta,\phi)=\frac{\partial\underline{\hat{x}}}{\partial\theta}=(\cos\theta\cos\phi,\cos\theta\sin\phi,-\sin\theta)^{\mathrm{T}},\quad 0\le\theta\le\pi,\quad 0\le\phi<2\pi, \tag{69}$$

$$\underline{\hat{x}}_{\phi}(\theta,\phi)=\frac{\partial\underline{\hat{x}}}{\partial\phi}=(-\sin\theta\sin\phi,\sin\theta\cos\phi,0)^{\mathrm{T}},\quad 0\le\theta\le\pi,\quad 0\le\phi<2\pi. \tag{70}$$

Furthermore, let us consider $\xi$ as an independent variable so that we can use the notation $O((\xi-1)^s)$, $s\ge 0$ when $\xi\to 1$. Working as in [11, Section 1, pp. 1830–1831], we derive the following expansions for the outward normal vector $\underline{n}(\underline{x})$, $\underline{x}\in\partial\Omega$ and for the free-space Green functions of the Helmholtz operator $\Phi_{\pm\frac{\omega}{c}}$,

$$\underline{n}(\xi(\underline{\hat{x}})\underline{\hat{x}})=\underline{\hat{x}}+\underline{\hat{x}}_{\theta}\sum_{s=1}^{+\infty}\mu_{s,\theta}(\underline{\hat{x}})+\underline{\hat{x}}_{\phi}\sum_{s=1}^{+\infty}\mu_{s,\phi}(\underline{\hat{x}}),\quad \underline{\hat{x}}\in\partial B, \tag{71}$$

$$\frac{\partial\,\cdot}{\partial\underline{n}(\xi(\underline{\hat{x}})\underline{\hat{x}})}=\frac{\partial\cdot}{\partial r}+\left(\sum_{s=0}^{+\infty}\mu_{s,\theta}(\underline{\hat{x}})\right)\frac{\partial\cdot}{\partial\theta}+\left(\sum_{s=0}^{+\infty}\mu_{s,\phi}(\underline{\hat{x}})\right)\frac{\partial\cdot}{\partial\phi},\quad \underline{\hat{x}}\in\partial B, \tag{72}$$

$$\Phi_{\pm\frac{\omega}{c}}(\|\underline{x}\|\underline{\hat{x}},\underline{y})=\sum_{s=0}^{+\infty}\frac{(\|\underline{x}\|-1)^s}{s!}\frac{\partial^s\Phi_{\pm\frac{\omega}{c}}(\underline{\hat{x}},\underline{y})}{\partial r^s},\quad \|\underline{x}\|>a,\ \underline{\hat{x}}\in\partial B,\ \underline{y}\in\partial B_a, \tag{73}$$

where $0!=1$ and $\mu_{s,\theta}=O((\xi-1)^s)$, $\mu_{s,\phi}=O((\xi-1)^s)$, $s\ge 0$, when $\xi\to 1$ (see [11, Section 1, pp. 1830–1831]). From formulae (43), (44), (48–51) of [11] we have

$$\begin{aligned}
&\mu_{0,\theta}(\underline{\hat{x}}(\theta,\phi))=\mu_{0,\phi}(\underline{\hat{x}}(\theta,\phi))=0,\quad 0\le\theta\le\pi,\ 0\le\phi<2\pi,\\
&\mu_{1,\theta}(\underline{\hat{x}}(\theta,\phi))=-\frac{\partial}{\partial\theta}\xi(\underline{\hat{x}}(\theta,\phi)),\quad 0\le\theta\le\pi,\ 0\le\phi<2\pi,\\
&\mu_{1,\phi}(\underline{\hat{x}}(\theta,\phi))=-\frac{1}{\sin^2\theta}\frac{\partial}{\partial\phi}\xi(\underline{\hat{x}}(\theta,\phi)),\quad 0\le\theta\le\pi,\ 0\le\phi<2\pi.
\end{aligned} \tag{74}$$

We note that, by using the Cauchy product rule to multiply the series and formulae (72) and (73), we can derive the series expansion in powers of $(\xi-1)$ of $\partial\Phi_{\pm\omega/c}/\partial\underline{n}$. Series (71) and (72) converge when $|\xi-1|<1$; series (73) converges when $\underline{\hat{x}}\in\partial B$ and $\underline{y}\in\partial B_a$ since $0<a<1$ and $\overline{B_a}\subset\Omega$. Finally, let us assume that, for $(\omega,\underline{\alpha})\in W_{N_1,N_2}$, the following series expansions in powers of $(\xi-1)$ hold for the density functions $\tilde{u}_{\omega,\underline{\alpha}}$, $\tilde{v}_{\omega,\underline{\alpha}}$ and for the function $f_\epsilon$ given in (25),

$$\tilde{u}_{\omega,\underline{\alpha}}(\underline{\hat{x}})=\sum_{s=0}^{+\infty}\frac{(\xi(\underline{\hat{x}})-1)^s}{s!}\tilde{u}_{s,\omega,\underline{\alpha}}(\underline{\hat{x}}),\quad \underline{\hat{x}}\in\partial B, \tag{75}$$

$$\tilde{v}_{\omega,\underline{\alpha}}(\underline{\hat{x}})=\sum_{s=0}^{+\infty}\frac{(\xi(\underline{\hat{x}})-1)^s}{s!}\tilde{v}_{s,\omega,\underline{\alpha}}(\underline{\hat{x}}),\quad \underline{\hat{x}}\in\partial B, \tag{76}$$

$$f_\epsilon(\underline{\hat{x}})=\sum_{s=0}^{+\infty}f_{\epsilon,s}(\underline{\hat{x}}),\quad \underline{\hat{x}}\in\partial B, \tag{77}$$

where $f_{\epsilon,s}=O((\xi-1)^s)$, $s\ge 0$; in particular, when $\xi\to 1$, we have:

$$f_{\epsilon,0}(\underline{\hat{x}})=(1+\epsilon)^2,\quad \underline{\hat{x}}\in\partial B, \tag{78}$$

$$f_{\epsilon,1}(\underline{\hat{x}})=2\epsilon(\epsilon+1)(\xi(\underline{\hat{x}})-1),\quad \underline{\hat{x}}\in\partial B, \tag{79}$$

$$f_{\epsilon,2}(\underline{\hat{x}})=(1+(\epsilon+1)(3\epsilon-1))(\xi(\underline{\hat{x}})-1)^2+0{\cdot}5(1-(\epsilon+1)^2)\times\left\{\left(\frac{\partial\xi}{\partial\theta}(\underline{\hat{x}})\right)^2+\frac{1}{\sin^2\theta}\left(\frac{\partial\xi}{\partial\phi}(\underline{\hat{x}})\right)^2\right\},\ \underline{\hat{x}}\in\partial B. \tag{80}$$

We note that formulae (73), (75), (76) imply the following expansions for $U_{\omega,\underline{\alpha}}$ and $V_{\omega,\underline{\alpha}}$,

$$U_{\omega,\underline{\alpha}}(\|\underline{x}\|\hat{\underline{x}}) = a^2 \sum_{s=0}^{+\infty} \sum_{\nu=0}^{s} \frac{(\|\underline{x}\|-1)^{s-\nu}}{(s-\nu)!} \int_{\partial B} \frac{\partial^{s-\nu} \Phi_{+\frac{\omega}{c}}}{\partial r^{s-\nu}}(\hat{\underline{x}}, a\hat{\underline{y}}) \tilde{u}_{\nu,\omega,\underline{\alpha}} \mathrm{d}s_{\partial B}(\hat{\underline{y}}), \quad \|\underline{x}\| > a, \ \hat{\underline{x}} \in \partial B, \tag{81}$$

and

$$V_{\omega,\underline{\alpha}}(\|\underline{x}\|\hat{\underline{x}}) = a^2 \sum_{s=0}^{+\infty} \sum_{\nu=0}^{s} \frac{(\|\underline{x}\|-1)^{s-\nu}}{(s-\nu)!} \int_{\partial B} \frac{\partial^{s-\nu} \Phi_{-\frac{\omega}{c}}}{\partial r^{s-\nu}}(\hat{\underline{x}}, a\hat{\underline{y}}) \tilde{v}_{\nu,\omega,\underline{\alpha}} \mathrm{d}s_{\partial B}(\hat{\underline{y}}), \quad \|\underline{x}\| > a, \ \hat{\underline{x}} \in \partial B. \tag{82}$$

Substituting (81), (82) in (66), (67) we obtain the following set of integral equations defined on $\partial B$ for the densities $\tilde{u}_{s,\omega,\underline{\alpha}}, \tilde{v}_{s,\omega,\underline{\alpha}}, (\omega,\underline{\alpha}) \in W_{N_1,N_2}, s = 0,1,\ldots,$

$$\begin{aligned} &\mathrm{i}\omega a^2 \int_{\partial B} \Phi_{+\frac{\omega}{c}}(\hat{\underline{x}}, a\hat{\underline{y}}) \tilde{u}_{s,\omega,\underline{\alpha}}(\hat{\underline{y}}) \mathrm{d}s_{\partial B}(\hat{\underline{y}}) + c\chi a^2 \int_{\partial B} \frac{\partial \Phi_{+\frac{\omega}{c}}}{\partial r}(\hat{\underline{x}}, a\hat{\underline{y}}) \tilde{u}_{s,\omega,\underline{\alpha}}(\hat{\underline{y}}) \mathrm{d}s_{\partial B}(\hat{\underline{y}}) \\ &\quad + \frac{(1+\chi)}{2\mu\varsigma} a^2 \int_{\partial B} \Phi_{-\frac{\omega}{c}}(\hat{\underline{x}}, a\hat{\underline{y}}) \tilde{v}_{s,\omega,\underline{\alpha}}(\hat{\underline{y}}) \mathrm{d}s_{\partial B}(\hat{\underline{y}}) = z_{s,\omega,\underline{\alpha}}(\hat{\underline{x}}), \hat{\underline{x}} \in \partial B, \quad (\omega,\underline{\alpha}) \in W_{N_1,N_2}, \ s = 0,1,\ldots, \end{aligned} \tag{83}$$

$$\begin{aligned} &\mathrm{i}\omega a^2 \int_{\partial B} \Phi_{-\frac{\omega}{c}}(\hat{\underline{x}}, a\hat{\underline{y}}) \tilde{v}_{s,\omega,\underline{\alpha}}(\hat{\underline{y}}) \mathrm{d}s_{\partial B}(\hat{\underline{y}}) - c\chi a^2 \int_{\partial B} \frac{\partial \Phi_{+\frac{\omega}{c}}}{\partial r}(\underline{x}, a\hat{\underline{y}}) \tilde{v}_{s,\omega,\underline{\alpha}}(\hat{\underline{y}}) \mathrm{d}s_{\partial B}(\hat{\underline{y}}) \\ &\quad + 2\lambda(1+\chi) I_K(\omega) f_{\epsilon,0}(\hat{\underline{x}}) a^2 \int_{\partial B} \Phi_{+\frac{\omega}{c}}((1+\epsilon)\hat{\underline{x}}, a\hat{\underline{y}}) \tilde{u}_{s,\omega,\underline{\alpha}}(\hat{\underline{y}}) \mathrm{d}s_{\partial B}(\hat{\underline{y}}) = z^*_{s,\omega,\underline{\alpha}}(\hat{\underline{x}}), \\ &\qquad \underline{x} = \xi(\hat{\underline{x}})\hat{\underline{x}} \in \partial\Omega, \ \hat{\underline{x}} \in \partial B, \ (\omega,\underline{\alpha}) \in W_{N_1,N_2}, \ s = 0,1,\ldots, \end{aligned} \tag{84}$$

where

$$z_{0,\omega,\underline{\alpha}}(\hat{\underline{x}}) = b_{\omega,\underline{\alpha}}(\xi(\hat{\underline{x}})\hat{\underline{x}}), \quad \hat{\underline{x}} \in \partial B, \ (\omega,\underline{\alpha}) \in W_{N_1,N_2}, \tag{85}$$

$$z^*_{0,\omega,\underline{\alpha}}(\hat{\underline{x}}) = 2\lambda(1+\chi) I_K(\omega) f_\epsilon(\hat{\underline{x}}) u^s_{G,\omega,\underline{\alpha}}(\xi(\hat{\underline{x}})\hat{\underline{x}} + \epsilon\hat{\underline{x}}), \quad \hat{\underline{x}} \in \partial B, \ (\omega,\underline{\alpha}) \in W_{N_1,N_2}, \tag{86}$$

and

$$\begin{aligned} z_{s,\omega,\underline{\alpha}}(\hat{\underline{x}}) = &-\mathrm{i}\omega a^2 \sum_{\nu=0}^{s-1} \frac{(\xi(\hat{\underline{x}})-1)^{s-\nu}}{(s-\nu)!} \int_{\partial B} \mathrm{d}s_{\partial B}(\hat{\underline{y}}) \frac{\partial^{s-\nu} \Phi_{+\frac{\omega}{c}}}{\partial r^{s-\nu}}(\hat{\underline{x}}, a\hat{\underline{y}}) \frac{(\xi(\hat{\underline{y}})-1)^{\nu}}{\nu!} \tilde{u}_{\nu,\omega,\underline{\alpha}}(\hat{\underline{y}}) \\ &- c\chi a^2 \sum_{\nu=0}^{s-1} \frac{(\xi(\hat{\underline{x}})-1)^{s-\nu}}{(s-\nu)!} \int_{\partial B} \mathrm{d}s_{\partial B}(\hat{\underline{y}}) \frac{\partial^{s-\nu+1} \Phi_{+\frac{\omega}{c}}}{\partial r^{s-\nu+1}}(\hat{\underline{x}}, a\hat{\underline{y}}) \frac{(\xi(\hat{\underline{y}})-1)^{\nu}}{\nu!} \tilde{u}_{\nu,\omega,\underline{\alpha}}(\hat{\underline{y}}) \\ &- c\chi a^2 \sum_{\nu=0}^{s-1} \sum_{p=0}^{\nu} \mu_{s-\nu,\theta}(\hat{\underline{x}}) \frac{(\xi(\hat{\underline{x}})-1)^{\nu-p}}{(\nu-p)!} \int_{\partial B} \mathrm{d}s_{\partial B}(\hat{\underline{y}}) \frac{\partial^{s-\nu+1} \Phi_{+\frac{\omega}{c}}}{\partial r^{s-\nu} \partial\theta}(\hat{\underline{x}}, a\hat{\underline{y}}) \frac{(\xi(\hat{\underline{y}})-1)^{p}}{p!} \tilde{u}_{p,\omega,\underline{\alpha}}(\hat{\underline{y}}) \\ &- c\chi a^2 \sum_{\nu=0}^{s-1} \sum_{p=0}^{\nu} \mu_{s-\nu,\phi}(\hat{\underline{x}}) \frac{(\xi(\hat{\underline{x}})-1)^{\nu-p}}{(\nu-p)!} \int_{\partial B} \mathrm{d}s_{\partial B}(\hat{\underline{y}}) \frac{\partial^{s-\nu+1} \Phi_{+\frac{\omega}{c}}}{\partial r^{s-\nu} \partial\phi}(\hat{\underline{x}}, a\hat{\underline{y}}) \frac{(\xi(\hat{\underline{y}})-1)^{p}}{p!} \tilde{u}_{p,\omega,\underline{\alpha}}(\hat{\underline{y}}) \\ &- \frac{(1+\chi)}{2\mu\varsigma} a^2 \sum_{\nu=0}^{s-1} \frac{(\xi(\hat{\underline{x}})-1)^{s-\nu}}{(s-\nu)!} \int_{\partial B} \mathrm{d}s_{\partial B}(\hat{\underline{y}}) \frac{\partial^{s-\nu} \Phi_{-\frac{\omega}{c}}}{\partial r^{s-\nu}}(\hat{\underline{x}}, a\hat{\underline{y}}) \frac{(\xi(\hat{\underline{y}})-1)^{\nu}}{\nu!} \tilde{v}_{\nu,\omega,\underline{\alpha}}(\hat{\underline{y}}), \\ &\hat{\underline{x}} \in \partial B, \ (\omega,\underline{\alpha}) \in W_{N_1,N_2}, \ s = 1,2,\ldots, \end{aligned} \tag{87}$$

$$\begin{aligned} z^*_{s,\omega,\underline{\alpha}}(\hat{\underline{x}}) = &-\mathrm{i}\omega a^2 \sum_{\nu=0}^{s-1} \frac{(\xi(\hat{\underline{x}})-1)^{s-\nu}}{(s-\nu)!} \int_{\partial B} \mathrm{d}s_{\partial B}(\hat{\underline{y}}) \frac{\partial^{s-\nu} \Phi_{-\frac{\omega}{c}}}{\partial r^{s-\nu}}(\hat{\underline{x}}, a\hat{\underline{y}}) \frac{(\xi(\hat{\underline{y}})-1)^{\nu}}{\nu!} \tilde{v}_{\nu,\omega,\underline{\alpha}}(\hat{\underline{y}}) \\ &+ c\chi a^2 \sum_{\nu=0}^{s-1} \frac{(\xi(\hat{\underline{x}})-1)^{s-\nu}}{(s-\nu)!} \int_{\partial B} \mathrm{d}s_{\partial B}(\hat{\underline{y}}) \frac{\partial^{s-\nu+1} \Phi_{-\frac{\omega}{c}}}{\partial r^{s-\nu+1}}(\hat{\underline{x}}, a\hat{\underline{y}}) \frac{(\xi(\hat{\underline{y}})-1)^{\nu}}{\nu!} \tilde{v}_{\nu,\omega,\underline{\alpha}}(\hat{\underline{y}}) \end{aligned}$$

$$+c\chi a^2\sum_{\nu=0}^{s-1}\sum_{p=0}^{\nu}\mu_{s-\nu,\theta}(\hat{\underline{x}})\frac{(\xi(\hat{\underline{x}})-1)^{\nu-p}}{(\nu-p)!}\int_{\partial B}\mathrm{d}s_{\partial B}(\hat{\underline{y}})\frac{\partial^{s-\nu+1}\Phi_{-\frac{\omega}{c}}}{\partial r^{s-\nu}\partial\theta}(\hat{\underline{x}},a\hat{\underline{y}})\frac{(\xi(\hat{\underline{y}})-1)^p}{p!}\tilde{v}_{p,\omega,\underline{\alpha}}(\hat{\underline{y}})$$

$$+c\chi a^2\sum_{\nu=0}^{s-1}\mu_{s-\nu,\phi}(\hat{\underline{x}})\sum_{p=0}^{\nu}\frac{(\xi(\hat{\underline{x}})-1)^{\nu-p}}{(\nu-p)!}\int_{\partial B}\mathrm{d}s_{\partial B}(\hat{\underline{y}})\frac{\partial^{s-\nu+1}\Phi_{-\frac{\omega}{c}}}{\partial r^{s-\nu}\partial\phi}(\hat{\underline{x}},a\hat{\underline{y}})\frac{(\xi(\hat{\underline{y}})-1)^p}{p!}\tilde{v}_{p,\omega,\underline{\alpha}}(\hat{\underline{y}})$$

$$-2\lambda I_K(\omega)(1+\chi)a^2\sum_{\nu=0}^{s-1}f_{\epsilon,s-\nu}(\hat{\underline{x}})\sum_{p=0}^{\nu}\frac{(\xi(\hat{\underline{x}})-1)^{\nu-p}}{(\nu-p)!}\cdot$$

$$\int_{\partial B}\mathrm{d}s_{\partial B}(\hat{\underline{y}})\frac{\partial^{\nu-p}\Phi_{+\frac{\omega}{c}}}{\partial r^{s-\nu}}((1+\epsilon)\hat{\underline{x}},a\hat{\underline{y}})\frac{(\xi(\hat{\underline{y}})-1)^p}{p!}\tilde{u}_{p,\omega,\underline{\alpha}}(\hat{\underline{y}}),\ \ \hat{\underline{x}}\in\partial B,\ \ (\omega,\underline{\alpha})\in W_{N_1,N_2},\ \ s=1,2,\ldots. \tag{88}$$

We note that when $\chi=0, K=\mathbb{R}, \epsilon=0$ and $u^s_{G,s,\omega,\underline{\alpha}}(\hat{\underline{x}})=0, \hat{\underline{x}}\in\partial B, (\omega,\underline{\alpha})\in W_{N_1,N_2}, s=0,1,\ldots,$ formulae (87) and (88) reduce to the formulae (88), (89) of [1]. Let $Y_{\sigma,l,m}(\hat{\underline{x}}), \hat{\underline{x}}\in\partial B, \sigma=0,1, l=\sigma,\sigma+1,\ldots, m=\sigma,\sigma+1,\ldots,l$ be the spherical harmonic functions (see [12, p. 77]) we have the following expansions for $\Phi_{\pm\frac{\omega}{c}}(\underline{x},\underline{y})$ (see [11, p. 1833]):

$$\Phi_{+\frac{\omega}{c}}(\underline{x},\underline{y})=\mathrm{i}\frac{\omega}{c}\sum_{\sigma=0}^{1}\sum_{l=\sigma}^{+\infty}\sum_{m=\sigma}^{l}h_l\left(\frac{\omega}{c}\|\underline{x}\|\right)j_l\left(\frac{\omega}{c}\|\underline{y}\|\right)Y_{\sigma,l,m}(\hat{\underline{x}})Y_{\sigma,l,m}(\hat{\underline{y}}),$$
$$\underline{x}=\|\underline{x}\|\hat{\underline{x}},\ \underline{y}=\|\underline{y}\|\hat{\underline{y}},\ \|\underline{x}\|>\|\underline{y}\|,\hat{\underline{y}},\ \hat{\underline{x}}\in\partial B, \tag{89}$$

$$\Phi_{-\frac{\omega}{c}}(\underline{x},\underline{y})=\overline{\Phi_{+\frac{\omega}{c}}(\underline{x},\underline{y})}=-\mathrm{i}\frac{\omega}{c}\sum_{\sigma=0}^{1}\sum_{l=\sigma}^{+\infty}\sum_{m=\sigma}^{l}\overline{h}_l\left(\frac{\omega}{c}\|\underline{x}\|\right)j_l\left(\frac{\omega}{c}\|\underline{y}\|\right)Y_{\sigma,l,m}(\hat{\underline{x}})Y_{\sigma,l,m}(\hat{\underline{y}}),$$
$$\underline{x}=\|\underline{x}\|\hat{\underline{x}},\ \ \underline{y}=\|\underline{y}\|\hat{\underline{y}},\ \ \|\underline{x}\|>\|\underline{y}\|,\ \hat{\underline{y}},\ \hat{\underline{x}}\in\partial B, \tag{90}$$

where $h_l(z)$, $j_l(z)$, $l=0,1,\ldots,$ are the spherical Hankel and Bessel functions, respectively (see [12, p. 76–79]), $\overline{h}_l$, $\overline{\Phi_{+\frac{\omega}{c}}}$ are the complex conjugates of $h_l$ and $\Phi_{+\frac{\omega}{c}}$, respectively, and $h_l'(z)$, $l=0,1,\ldots$ are the derivatives with respect to $z$ of the function $h_l(z), l=0,1,\ldots.$

Let us define the following quantities:

$$d_{\omega,l}=-\mathrm{i}\omega h_l\left(\frac{\omega}{c}\right)-\chi\omega h_l'\left(\frac{\omega}{c}\right),\quad l=0,1,\ldots,\ \omega\in\mathbb{R}, \tag{91}$$

and

$$r_{\omega,l}=-|d_{\omega,l}|^2-\frac{\lambda I_K(\omega)}{\mu}(1+\chi)^2(1+\epsilon)^2h_l\left((1+\epsilon)\frac{\omega}{c}\right)\overline{h_l}\left(\frac{\omega}{c}\right),\quad l=0,1,\ldots,\ \omega\in\mathbb{R}, \tag{92}$$

for $(\omega,\underline{\alpha})\in W_{N_1,N_2}$; we denote by $z_{s,\omega,\underline{\alpha},\sigma,l,m}$, $z^*_{s,\omega,\underline{\alpha},\sigma,l,m}$, $\sigma=0,1$, $l=\sigma,\sigma+1,\ldots,m=\sigma,\sigma+1,\ldots,l$ the generalized Fourier coefficients of the functions $z_{s,\omega,\underline{\alpha}}$ and $z^*_{s,\omega,\underline{\alpha}}$, $s=0,1,\ldots$ defined in (87), (88) respectively, that is:

$$z_{s,\omega,\underline{\alpha},\sigma,l,m}=\int_{\partial B}Y_{\sigma,l,m}(\hat{\underline{x}})z_{s,\omega,\underline{\alpha}}(\hat{\underline{x}})\mathrm{d}s_{\partial B}(\hat{\underline{x}}),$$
$$z^*_{s,\omega,\underline{\alpha},\sigma,l,m}=\int_{\partial B}Y_{\sigma,l,m}(\hat{\underline{x}})z^*_{s,\omega,\underline{\alpha}}(\hat{\underline{x}})\mathrm{d}s_{\partial B}(\hat{\underline{x}}), \tag{93}$$
$$(\omega,\underline{\alpha})\in W_{N_1,N_2},\ s=0,1,\ldots,\ \sigma=0,1,l=\sigma,\sigma+1,\ldots,\ m=\sigma,\sigma+1,\ldots,l.$$

For $(\omega,\underline{\alpha}) \in W_{N_1,N_2}$, using the basis of the spherical harmonic functions from (65), (63), (89) and (90), we obtain:

$$U_{\omega,\underline{\alpha}}(\|\underline{x}\|\underline{\hat{x}}) = \sum_{\sigma=0}^{1}\sum_{l=\sigma}^{+\infty}\sum_{m=\sigma}^{l} \tilde{u}^*_{\omega,\underline{\alpha},\sigma,l,m} h_l\left(\frac{\omega\|\underline{x}\|}{c}\right) Y_{\sigma,l,m}(\underline{\hat{x}}), \quad \|\underline{x}\| > a,\ \underline{\hat{x}} \in \partial B,\ (\omega,\underline{\alpha}) \in W_{N_1,N_2}, \tag{94}$$

$$V_{\omega,\underline{\alpha}}(\|\underline{x}\|\underline{\hat{x}}) = \sum_{\sigma=0}^{1}\sum_{l=\sigma}^{+\infty}\sum_{m=\sigma}^{l} \tilde{v}^*_{\omega,\underline{\alpha},\sigma,l,m} h_l\left(\frac{\omega\|\underline{x}\|}{c}\right) Y_{\sigma,l,m}(\underline{\hat{x}}), \quad \|\underline{x}\| > a,\ \underline{\hat{x}} \in \partial B,\ (\omega,\underline{\alpha}) \in W_{N_1,N_2}, \tag{95}$$

where $\tilde{u}^*_{\omega,\underline{\alpha},\sigma,l,m}$, $\tilde{v}^*_{\omega,\underline{\alpha},\sigma,l,m}$, $\sigma = 0,1$, $l = \sigma,\sigma+1,\ldots,m = \sigma,\sigma+1,\ldots,l$, $s = 0,1,\ldots$ are the generalized Fourier coefficients of the functions $U_{\omega,\underline{\alpha}}(\underline{\hat{x}})$, $V_{\omega,\underline{\alpha}}(\underline{\hat{x}})$, $\underline{\hat{x}} \in \partial B$. From formulae (94), (95) and (81), (82), we obtain:

$$\begin{aligned}
\tilde{u}^*_{\omega,\underline{\alpha},\sigma,l,m} &= \sum_{s=0}^{+\infty} a^2 \int_{\partial B} \mathrm{d}s_{\partial B}(\underline{\hat{x}}) Y_{\sigma,l,m}(\underline{\hat{x}}) \int_{\partial B} \mathrm{d}s_{\partial B}(\underline{\hat{y}}) \Phi_{+\frac{\omega}{c}}(\underline{\hat{x}}, a\underline{\hat{y}}) \tilde{u}_{s,\omega,\underline{\alpha}}(\underline{\hat{y}}) \\
&= \sum_{s=0}^{+\infty} \mathrm{i}\left(\frac{\omega}{c}\right) h_l\left(\frac{\omega}{c}\right) j_l\left(\frac{a\omega}{c}\right) a^2 \int_{\partial B} \mathrm{d}s_{\partial B}(\underline{\hat{y}}) Y_{\sigma,l,m}(\underline{\hat{y}}) \tilde{u}_{s,\omega,\underline{\alpha}}(\underline{\hat{y}}), \\
&\quad (\omega,\underline{\alpha}) \in W_{N_1,N_2},\ \sigma = 0,1, l = \sigma,\sigma+1,\ldots,\ m = \sigma,\sigma+1,\ldots,l,
\end{aligned} \tag{96}$$

and

$$\begin{aligned}
\tilde{v}^*_{\omega,\underline{\alpha},\sigma,l,m} &= \sum_{s=0}^{+\infty} a^2 \int_{\partial B} \mathrm{d}s_{\partial B}(\underline{\hat{x}}) Y_{\sigma,l,m}(\underline{\hat{x}}) \int_{\partial B} \mathrm{d}s_{\partial B}(\underline{\hat{y}}) \Phi_{-\frac{\omega}{c}}(\underline{\hat{x}}, a\underline{\hat{y}}) \tilde{v}_{s,\omega,\underline{\alpha}}(\underline{\hat{y}}) \\
&= -\sum_{s=0}^{+\infty} \mathrm{i}\left(\frac{\omega}{c}\right) \overline{h_l}\left(\frac{\omega}{c}\right) j_l\left(\frac{a\omega}{c}\right) a^2 \int_{\partial B} \mathrm{d}s_{\partial B}(\underline{\hat{y}}) Y_{\sigma,l,m}(\underline{\hat{y}}) \tilde{v}_{s,\omega,\underline{\alpha}}(\underline{\hat{y}}), \\
&\quad (\omega,\underline{\alpha}) \in W_{N_1,N_2},\ \sigma = 0,1, l = \sigma,\sigma+1,\ldots,\ m = \sigma,\sigma+1,\ldots,l.
\end{aligned} \tag{97}$$

Using formulae (89) and (90) and Equations (83), (84), we obtain the quantities:
$j_l(a\omega/c)a^2 \int_{\partial B} \mathrm{d}s_{\partial B}(\underline{\hat{y}}) Y_{\sigma,l,m}(\underline{\hat{y}}) \tilde{u}_{s,\omega,\underline{\alpha}}(\underline{\hat{y}})$ and $j_l(a\omega/c)a^2 \int_{\partial B} \mathrm{d}s_{\partial B}(\underline{\hat{y}}) Y_{\sigma,l,m}(\underline{\hat{y}}) \tilde{v}_{s,\omega,\underline{\alpha}}(\underline{\hat{y}})$, $(\omega,\underline{\alpha}) \in W_{N_1,N_2}$, $s = 0,1,\ldots$, $\sigma = 0,1$, $l = \sigma,\sigma+1,\ldots$, $m = \sigma,\sigma+1,\ldots,l$ and we derive the following expressions for the coefficients $\tilde{u}^*_{\omega,\underline{\alpha},\sigma,l,m}$, $\tilde{v}^*_{\omega,\underline{\alpha},\sigma,l,m}$, $(\omega,\underline{\alpha}) \in W_{N_1,N_2}$, $\sigma = 0,1$, $l = \sigma,\sigma+1,\ldots,m = \sigma,\sigma+1,\ldots,l$:

$$\begin{aligned}
\tilde{u}^*_{\omega,\underline{\alpha},\sigma,l,m} &= \sum_{s=0}^{+\infty} \frac{-\overline{d_{\omega,l}} z_{s,\omega,\underline{\alpha},\sigma,l,m} + (1+\chi)\overline{h_l}(\frac{\omega}{c}) z^*_{s,\omega,\underline{\alpha},\sigma,l,m}/(2\mu)}{r_{\omega,l}}, \\
&\quad (\omega,\underline{\alpha}) \in W_{N_1,N_2}, \sigma = 0,1,\ l = \sigma,\sigma+1,\ldots,\ m = \sigma,\sigma+1,\ldots,l,
\end{aligned} \tag{98}$$

$$\begin{aligned}
\tilde{v}^*_{\omega,\underline{\alpha},\sigma,l,m} &= \sum_{s=0}^{+\infty} \frac{d_{\omega,l} z^*_{s,\omega,\underline{\alpha},\sigma,l,m} + 2\lambda I_K(\omega)(1+\chi)(1+\epsilon)^2 h_l(\frac{\omega}{c}(1+\epsilon)) z_{s,\omega,\underline{\alpha},\sigma,l,m}}{r_{\omega,l}} \\
&\quad (\omega,\underline{\alpha}) \in W_{N_1,N_2}, \sigma = 0,1,\ l = \sigma,\sigma+1,\ldots,\ m = \sigma,\sigma+1,\ldots,l.
\end{aligned} \tag{99}$$

We conclude this section by noting that the computation of the coefficients $\tilde{u}^*_{\omega,\underline{\alpha},\sigma,l,m}$, $\tilde{v}^*_{\omega,\underline{\alpha},\sigma,l,m}$, $(\omega,\underline{\alpha}) \in W_{N_1,N_2}$, $\sigma = 0,1$, $l = \sigma,\sigma+1,\ldots,m = \sigma,\sigma+1,\ldots,l$ is highly parallelizable since it requires the computation of the integrals contained in formula (93). Each integral is independent from the others, and the computation can be carried out in parallel. Furthermore, each of these integrals can be computed in parallel; in fact, the integrals are approximated by Riemann sums and the computation of Riemann sums is easily parallelizable.

## 4 Numerical results

In this section, we present numerical results obtained on test problems with a parallel implementation of the numerical methods introduced in Section 3. The codes have been written in Fortran 77 using MPI for message passing, and were tested on an SP4 machine with 512 processors of the Cineca (Casalecchio di Reno, BO), Italy computer center.

We validate the mathematical models and the numerical methods presented in the previous sections for two test problems: the first one relates to the definite-band furtivity problem, and the second relates to the definite-band ghost-obstacle problem. The results obtained are discussed both from a quantitative and a qualitative point of view. In the numerical experiments, we denote by $u_a^s$ the wave scattered by the smart obstacle (i.e., the active obstacle) and by $u_p^s$ the wave scattered by the passive obstacle. Moreover, we provide a quantitative basis to the attempt made by the smart obstacle to hide its real nature (shape, impedance, location) through the performance indices $i_{F,K}$, $\tilde{i}_{F,K}$, $\breve{i}_{F,K}$, relative to the furtivity problem, and $i_{G,K}$, $\tilde{i}_{G,K}$, $\breve{i}_{G,K}$, relative to the ghost-obstacle problem, defined later.

The results contained in the tables and in the figures of this section show that the definite-band furtivity problem is "easier" than the definite-band ghost-obstacle problem. In fact, for given values of $\lambda$, $\mu$, $\varsigma$ and for a given set $K$ the solution of the control problems proposed gives more satisfactory results (i.e., $i_{F,K} > i_{G,K}$) in the case of the definite-band furtivity problem than in the case of the definite-band ghost-obstacle problem. Furthermore, the cost paid in terms of the control variable $\psi$ (i.e., the quantity $\int_{\mathbb{R}} \mathrm{d}t \int_{\partial\Omega} \mathrm{d}s_{\partial\Omega}(\underline{x})\psi^2(\underline{x},t)$ see (9)) to obtain the same value of $i_{F,K}$ and of $i_{G,K}$ is higher for $i_{G,K}$, that is, when we solve the definite-band ghost-obstacle problem, than for $i_{F,K}$, that is, when we solve the definite-band furtivity problem. Another observed phenomenon is that, in both problems (definite-band furtivity and definite-band ghost-obstacle), when we increase the "size" of the band $K$ (i.e., when we consider a new band $K_1 \supset K$), we spend more in terms of $\psi$ as shown in Tables 1, 3. Finally we show the quantitative character of the series expansions (94), (95) relative to the definite-band ghost-obstacle problem. A similar study to establish the quantitative character of the analogous series expansion relative to the furtivity problem (i.e., $K = \mathbb{R}$) can be found in [1].

**Table 1** Experiment 1: double cone, $\chi = 0$, incident wave (100) with $q = 1$

| $K$ | $i_{F,K}$ | $\tilde{i}_{F,K}$ | $C_{\psi,K}$ | $\tilde{i}_{F,K}/C_{\psi,K}$ | $\breve{i}_{F,\mathbb{R}\setminus K}$ |
|---|---|---|---|---|---|
| $\lambda = 0{\cdot}5, \mu = 0{\cdot}5, \varsigma = 1$ | | | | | |
| $(-0{\cdot}5, 0{\cdot}5)$ | 0·9433942 | 0·9444603 | 0·113029 | 8·3559 | $9{\cdot}937\times10^{-9}$ |
| $(-1, 1)$ | 0·736758 | 0·76687 | 0·5154179 | 1·48786 | $9{\cdot}970\times10^{-9}$ |
| $(-1{\cdot}5, 1{\cdot}5)$ | 0·595999 | 0·671255 | 0·54696733 | 1·22723 | $3{\cdot}073\times10^{-8}$ |
| $(-2, 2)$ | 0·5081838 | 0·608074 | 0·5263606 | 1·155242 | $3{\cdot}155\times10^{-8}$ |
| $(-2{\cdot}5, 2{\cdot}5)$ | 0·5324 | 0·577030 | 0·50925527 | 1·13308 | $3{\cdot}975\times10^{-8}$ |
| $(-3, 3)$ | 0·54551901 | 0·5667251 | 0·4979747 | 1·13806 | $4{\cdot}199\times10^{-8}$ |
| $(-4, 4)$ | 0·548331 | 0·5663212 | 0·49589065 | 1·1420 | $7{\cdot}005\times10^{-8}$ |
| $\mathbb{R}$ | 0·549079 | 0·5663196 | 0·49581666 | 1·1421 | 0 |
| $\lambda = 0{\cdot}9, \quad \mu = 0{\cdot}1, \quad \varsigma = 1$ | | | | | |
| $(-0{\cdot}5, 0{\cdot}5)$ | 0·993152 | 0·9932864 | 0·1228035 | 8·088421 | $9{\cdot}937\times10^{-9}$ |
| $(-1, 1)$ | 0·954775 | 0·96055673 | 0·7206326 | 1·325 | $9{\cdot}970\times10^{-9}$ |
| $(-1{\cdot}5, 1{\cdot}5)$ | 0·9119264 | 0·93127934 | 0·84401163 | 1·029548 | $3{\cdot}073\times10^{-8}$ |
| $(-2, 2)$ | 0·8691442 | 0·90347241 | 0·877712203 | 1·029349 | $3{\cdot}155\times10^{-8}$ |
| $(-2{\cdot}5, 2{\cdot}5)$ | 0·862403269 | 0·88381619 | 0·858445068 | 1·029548 | $3{\cdot}975\times10^{-8}$ |
| $(-3, 3)$ | 0·864009748 | 0·872720453 | 0·81426169 | 1·0717936 | $4{\cdot}199\times10^{-8}$ |
| $(-4, 4)$ | 0·861688 | 0·8715459 | 0·7979112102 | 1·0922843 | $7{\cdot}005\times10^{-8}$ |
| $\mathbb{R}$ | 0·86113615 | 0·8715627 | 0·7968449 | 1·0937671 | 0 |

**Table 2** Experiment 1: double cone, $\chi = 0$, incident wave (100) with $q = 2$

| $K$ | $i_{F,K}$ | $\tilde{i}_{F,K}$ | $C_{\psi,K}$ | $\tilde{i}_{F,K}/C_{\psi,K}$ | $\check{i}_{F,\mathbb{R}\setminus K}$ |
|---|---|---|---|---|---|
| $\lambda = 0{\cdot}5, \mu = 0{\cdot}5, \varsigma = 1$ | | | | | |
| $(-1,1)$ | 0·809381 | 0·8229476 | 848·5246 | $9{\cdot}699\times10^{-4}$ | $9{\cdot}52406\times10^{-8}$ |
| $(-2,2)$ | 0·228168 | 0·50047 | 3209·559 | $1{\cdot}559\times10^{-4}$ | $6{\cdot}1104242\times10^{-8}$ |
| $(-3,3)$ | 0·295004 | 0·411742 | 3961·48 | $1{\cdot}042\times10^{-4}$ | $6{\cdot}70722\times10^{-8}$ |
| $(-4,4)$ | 0·340357 | 0·397362 | 4469·48 | $8{\cdot}890\times10^{-5}$ | $6{\cdot}237531\times10^{-8}$ |
| $\lambda = 0{\cdot}9,\ \mu = 0{\cdot}1,\ \varsigma = 1$ | | | | | |
| $(-1,1)$ | 0·971426 | 0·973760 | 1124·7696 | $8{\cdot}657\times10^{-4}$ | $9{\cdot}52406\times10^{-8}$ |
| $(-2,2)$ | 0·738203 | 0·855474 | 7292·7085 | $1{\cdot}173\times10^{-4}$ | $6{\cdot}1104242\times10^{-8}$ |
| $(-3,3)$ | 0·683465 | 0·776248 | 10822·7369 | $7{\cdot}172\times10^{-5}$ | $6{\cdot}70722\times10^{-8}$ |
| $(-4,4)$ | 0·704218 | 0·739362 | 13890·872 | $5{\cdot}323\times10^{-5}$ | $6{\cdot}237531\times10^{-8}$ |

**Table 3** Convergence of the series expansions (94) and (95)

| $\frac{\omega}{c}$ | $\varepsilon^1_{u^s}$ | $\varepsilon^2_{u^s}$ | $\varepsilon^3_{u^s}$ | $\varepsilon^4_{u^s}$ | $\varepsilon^5_{u^s}$ | $\varepsilon^6_{u^s}$ | $\varepsilon^7_{u^s}$ | $\varepsilon^8_{u^s}$ |
|---|---|---|---|---|---|---|---|---|
| 1·0 | $2{\cdot}38\times10^{-2}$ | $4{\cdot}45\times10^{-4}$ | $4{\cdot}56\times10^{-2}$ | $2{\cdot}69\times10^{-3}$ | $1{\cdot}04\times10^{-4}$ | $2{\cdot}13\times10^{-3}$ | $2{\cdot}04\times10^{-4}$ | $1{\cdot}18\times10^{-5}$ |
| 2·0 | $2{\cdot}40\times10^{-2}$ | $9{\cdot}42\times10^{-4}$ | $4{\cdot}56\times10^{-2}$ | $3{\cdot}06\times10^{-3}$ | $1{\cdot}88\times10^{-4}$ | $2{\cdot}14\times10^{-3}$ | $2{\cdot}46\times10^{-4}$ | $2{\cdot}10\times10^{-5}$ |
| 3·0 | $2{\cdot}41\times10^{-2}$ | $1{\cdot}42\times10^{-3}$ | $4{\cdot}558\times10^{-2}$ | $3{\cdot}57\times10^{-3}$ | $2{\cdot}93\times10^{-3}$ | $2{\cdot}15\times10^{-3}$ | $3{\cdot}03\times10^{-4}$ | $3{\cdot}36\times10^{-5}$ |
| $\frac{\omega}{c}$ | $\varepsilon^1_{\varphi}$ | $\varepsilon^2_{\varphi}$ | $\varepsilon^3_{\varphi}$ | $\varepsilon^4_{\varphi}$ | $\varepsilon^5_{\varphi}$ | $\varepsilon^6_{\varphi}$ | $\varepsilon^7_{\varphi}$ | $\varepsilon^8_{\varphi}$ |
| 1·0 | $4{\cdot}88\times10^{-2}$ | $2{\cdot}64\times10^{-3}$ | $2{\cdot}57\times10^{-2}$ | $2{\cdot}97\times10^{-3}$ | $2{\cdot}06\times10^{-4}$ | $1{\cdot}19\times10^{-3}$ | $1{\cdot}82\times10^{-4}$ | $1{\cdot}57\times10^{-5}$ |
| 2·0 | $5{\cdot}07\times10^{-2}$ | $1{\cdot}34\times10^{-3}$ | $1{\cdot}72\times10^{-2}$ | $1{\cdot}41\times10^{-3}$ | $9{\cdot}55\times10^{-5}$ | $8{\cdot}03\times10^{-4}$ | $1{\cdot}01\times10^{-4}$ | $8{\cdot}89\times10^{-5}$ |
| 3·0 | $5{\cdot}69\times10^{-2}$ | $5{\cdot}68\times10^{-3}$ | $2{\cdot}08\times10^{-2}$ | $3{\cdot}67\times10^{-3}$ | $4{\cdot}32\times10^{-4}$ | $9{\cdot}84\times10^{-4}$ | $2{\cdot}29\times10^{-4}$ | $3{\cdot}31\times10^{-5}$ |

In the two experiments proposed here, we consider an incoming acoustic field of the following form:

$$u^i(\underline{x},t) = \mathrm{e}^{-q^2[(\underline{\gamma},\underline{x})-ct]^2}, \quad (\underline{x},t) \in \mathbb{R}^3 \times \mathbb{R}, \tag{100}$$

where $\underline{\gamma} \in \partial B$, $q$ is a positive constant and $c$ is the wave-propagation velocity. In the numerical experiments, we always choose $c$ and $\varsigma$ equal to one. Note that, owing to the choice (100) of the incident field, the approximation of $u^i$, $u^s$ and $\varphi$ with time-harmonic waves given in (51), (52) and (53) can be done by choosing: $N_2 = 1$, $\underline{\alpha}_1 = \underline{\gamma}$ and $a_{i,1}$, $\omega_i/(2qc)$, $i = 1,2,\ldots,N_1$ as the weights and the nodes of the Gauss–Hermite quadrature rule. In the numerical experiments discussed here we choose $N_1 = 400$. The motivation of this choice can be found in [11, Eq. (89)]. Finally, we denote by $U^{L_{\max},S}_{\omega,\underline{\alpha}}$ and $V^{L_{\max},S}_{\omega,\underline{\alpha}}$ the approximations of $U_{\omega,\underline{\alpha}}$ and $V_{\omega,\underline{\alpha}}$ obtained by truncating the series expansions in (94), (95) at $l = L_{\max}$ and the series expansion in (98), (99) at $s = S$, that is,

$$U^{L_{\max},S}_{\omega,\underline{\alpha}}(\|\underline{x}\|\hat{\underline{x}}) = \sum_{\sigma=0}^{1}\sum_{l=\sigma}^{L_{\max}}\sum_{m=\sigma}^{l} \tilde{u}^{*,S}_{\omega,\underline{\alpha},\sigma,l,m} h_l\left(\frac{\omega\|\underline{x}\|}{c}\right) Y_{\sigma,l,m}(\hat{\underline{x}}), \quad \|\underline{x}\| > a,\ \hat{\underline{x}} \in \partial B, \tag{101}$$

$$V^{L_{\max},S}_{\omega,\underline{\alpha}}(\|\underline{x}\|\hat{\underline{x}}) = \sum_{\sigma=0}^{1}\sum_{l=\sigma}^{L_{\max}}\sum_{m=\sigma}^{l} \tilde{v}^{S,*}_{\omega,\underline{\alpha},\sigma,l,m} h_l\left(\frac{\omega\|\underline{x}\|}{c}\right) Y_{\sigma,l,m}(\hat{\underline{x}}), \quad \|\underline{x}\| > a,\ \hat{\underline{x}} \in \partial B, \tag{102}$$

and with $u^s_{a,L_{\max},S}$, $\varphi_{L_{\max},S}$ the approximations of $u^s_a$ and $\varphi$ obtained using (101) and (102) in Eqs. (52) and (53), respectively. Using formulae similar to (101) and (52) (see [11]) we can approximate $u^s_p$ and $u^s_G$ with $u^s_{p,L_{\max},S}$ and $u^s_{G,L_{\max},S}$. In the numerical experiments discussed here, we choose $L_{\max} = 16$ in all experiments, and $S$ ranging between 1 and 8. A detailed discussion on the appropriate way of choosing these parameters can be found in [1, 11].

We now describe the definite-band furtivity experiment. The obstacle $(\Omega;\chi)$ is chosen to be an acoustically soft double cone. We recall that acoustically soft obstacles correspond to the choice $\chi = 0$. A double cone consists of two cones with a circular basis of radius 1·2 of the same height equal to $1 \cdot 2$ placed upon one another with common bases contained in the plane $x_3 = 0$ and centered in the origin (see Fig. 1a)). We choose an incident wave of the form (100) having $\underline{\gamma} = (0,0,-1)^{\mathrm{T}}$ and $q = 1$ (in Table 1) or $q = 2$ (in Table 2) and we choose $S = 4$.

Let us introduce the quantity $i_{F,K}$. Let $t_\nu = 0{\cdot}2(\nu-1)$, $\nu = 1,2,\ldots,10$ be 10 times and $\partial B_{R_i}, r_i = 1{\cdot}5+0{\cdot}5\ i$, $i = 1,2,\ldots,5$ be 5 spheres on which we want to compute the scattered fields $u^s_{a,L_{\max},S}$, $u^s_{p,L_{\max},S}$. We define for $\nu = 1,2,\ldots,10$ and $i = 1,2,\ldots,5$ the following quantities:

$$\epsilon^a_{F,K,i}(t_\nu) = \int_{\partial B_{R_i}} \left| \int_{\mathbb{R}} \mathrm{d}\tau\ \check{I}_K(\tau) u^s_{a,L_{\max},S}(\underline{x}, t_\nu - \tau) \right|^2 \mathrm{d}s_{\partial B_{R_i}}(\underline{x}), \tag{103}$$

$$\epsilon^p_{F,K,i}(t_\nu) = \int_{\partial B_{R_i}} \left| \int_{\mathbb{R}} \mathrm{d}\tau\ \check{I}_K(\tau) u^s_{p,L_{\max},S}(\underline{x}, t_\nu - \tau) \right|^2 \mathrm{d}s_{\partial B_{R_i}}(\underline{x}), \tag{104}$$

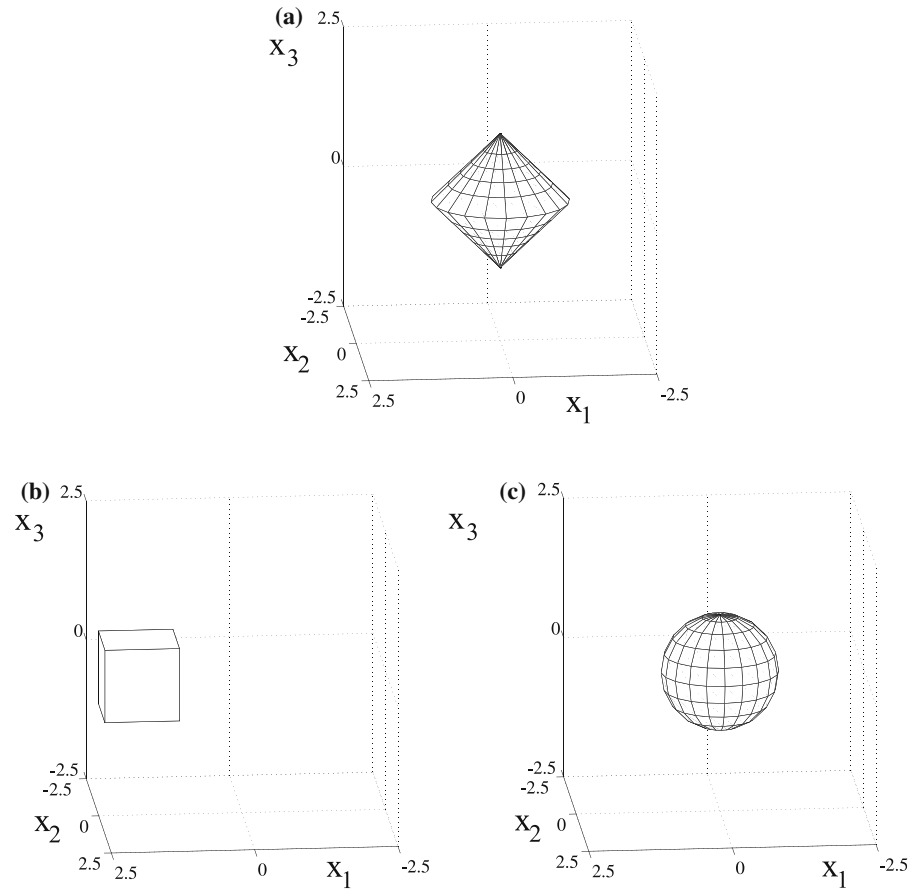


**Fig. 1** Obstacles of the furtivity (**a**) and ghost-obstacle problem (**b**), (**c**)

and finally we define

$$i_{F,K} = \min_{\substack{\nu=1,2,\ldots,10,\\ i=1,2,\ldots,5}} \frac{|\epsilon^p_{F,K,i}(t_\nu) - \epsilon^a_{F,K,i}(t_\nu)|}{\epsilon^p_{F,K,i}(t_\nu)}. \tag{105}$$

$$\tilde{i}_{F,K} = \frac{1}{50}\sum_{\nu=1}^{10}\sum_{i=1}^{5}\left\{\frac{|\epsilon^p_{F,K,i}(t_\nu) - \epsilon^a_{F,K,i}(t_\nu)|}{\epsilon^p_{F,K,i}(t_\nu)}\right\}. \tag{106}$$

The quantity $i_{F,K}$ measures the worst furtivity effect observed at times $t_\nu$, $\nu = 1,2,\ldots,10$ on the spheres $\partial B_{R_i}$, $i = 1,2,\ldots,5$, while the quantity $\tilde{i}_{F,K}$ measures a mean behavior of the furtivity effect under the same circumstances. Note that, when the convolution with respect to the time variable of $\check{I}_K$ and $u^s_{a,L_{\max},S}$, denoted by $\check{I}_K * u^s_{a,L_{\max},S}$ as done in (62), is equal to zero, that is, when the smart obstacle is completely undetectable in the frequency band $K$, the values of $i_{F,K}$ and $\tilde{i}_{F,K}$ will be equal to one. Similarly, when $\check{I}_K * u^s_{a,L_{\max},S} = \check{I}_K * u^s_{p,L_{\max},S}$, that is when there is no attempt to be furtive in the frequency band $K$, we have $i_{F,K}$ and $\tilde{i}_{F,K}$ equal to zero. Hence, values of $i_{F,K}$ and of $\tilde{i}_{F,K}$ close to unity indicate a satisfactory furtivity effect on the set $K$.

Finally, we denote by $\check{i}_{F,\mathbb{R}\setminus K}$ the quantity obtained from formulae (103)–(105) when we replace $K$ with $\mathbb{R}\setminus K$ and min with max. This last quantity measures the best furtivity effect obtained outside the frequency band $K$. As shown in Table 1, this effect is almost equal to zero. Furthermore, we denote by $C_{\psi,K}$ the quantity defined by

$$C_{\psi,K} = \sqrt{\frac{1}{10}\sum_{\nu=1}^{10}\int_{\partial\Omega}\left|\frac{1}{2\mu}\varphi_{L_{\max},S}(\underline{x},t_\nu)\right|^2 \mathrm{d}s_{\partial\Omega}(\underline{x})}. \tag{107}$$

The quantity $C_{\psi,K}$ measures the cost of minimization of the cost functional paid in terms of the control variable $\psi$. In fact, $\varphi_{L_{\max},S}(\underline{x},t)$ approximates $\tilde{\varphi}(\underline{x},t)$, and the relation between $\tilde{\varphi}$ and $\tilde{\psi}$ is given by (28). Recall that we have chosen $\varsigma = 1$.

Table 1 shows the behavior of $i_{F,K}$, $\tilde{i}_{F,K}$, $C_\psi$ and $\check{i}_{\mathbb{R}\setminus K}$ for several choices of the set $K$ and for two choices of the parameter $\lambda$. Several conclusions can be drawn and confirmed by the second experiment concerning the definite-band ghost-obstacle problem (see Table 3). First, as expected, when $\lambda$ increases, the furtivity effect in the worst case, measured by $i_{F,K}$, or in the mean case, measured by $\tilde{i}_{F,K}$, increases. In fact, when $\lambda = 0{\cdot}5$, the worst furtivity effect is about 50%, and when $\lambda = 0{\cdot}9$ it is about 86%. Furthermore, in general, we observe that, if we fix the value of $\lambda$ when the "size" of the set $K$ increases, the mean furtivity effect $\tilde{i}_{F,K}$ decreases and the cost in terms of $\psi$ paid to have a given furtivity effect, that is, for a fixed value of $\tilde{i}_{F,K}$, increases. In fact, the ratio $\tilde{i}_{F,K}/C_{\psi,K}$ gives the furtivity effect at unit cost in terms of $\psi$ that we must pay; when $K$ increases in size, the furtivity effect at unit cost in terms of $\psi$ decreases. For example, when $\lambda = 0{\cdot}5$, we can see that passing from $K = (-0{\cdot}5, 0{\cdot}5)$ to $K = (-2,2)$ the cost paid in terms of $\psi$ increases by a factor of about 8 (see the behavior of the ratio $\tilde{i}_{F,K}/C_{\psi,K}$). We note that, when the set $K$ passes from $(-2{\cdot}5, 2{\cdot}5)$ to $(-4,4)$, the furtivity effect remains substantially unchanged. This is probably due to the main part of the Fourier transform of the incoming field having support contained in $(-2{\cdot}5, 2{\cdot}5)$, so that passing from $K = (-2{\cdot}5, 2{\cdot}5)$ to $K = (-4,4)$ does not change substantially the problem considered. In order to investigate this behavior, we show in Table 2 results obtained under the circumstances of the experiment shown in Table 1, when the incoming wave is of the form given in (100) with $q = 2$.

Table 2 shows that the quantity $\tilde{i}_{F,K}$ increases when the size of $K$ decreases. Furthermore, in this case (i.e., $q = 2$) the cost measured by $C_{\psi,K}$ to be paid for solving the control problem is much higher than the cost to be paid in the case $q = 1$. This is reasonable since, when $q$ increases, the associated scattering problem becomes more difficult. In fact, in this case the relevance of high frequencies in the Fourier transform of the incident wave as a consequence of the scattered waves increases.

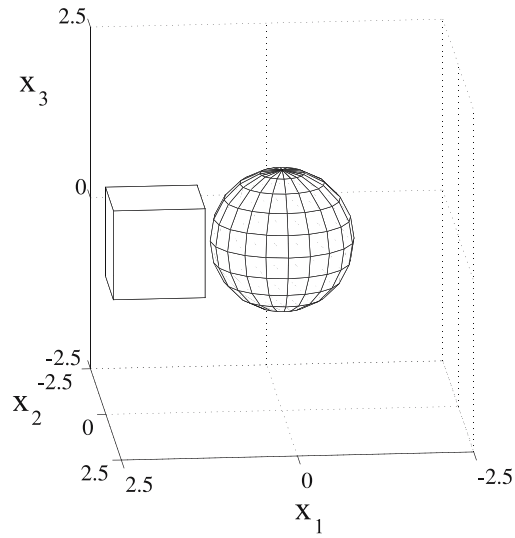


**Fig. 2** The setting of the ghost-obstacle problem. The sphere is the smart obstacle, and the cube is the ghost obstacle

We now describe the second experiment concerning the definite-band ghost-obstacle problem. The obstacle $(\Omega;\chi)$ is a sphere with center in the origin and radius $R = 1{\cdot}02$ with $\chi = 1$ (see Figure 1 c). The ghost $(\Omega_G;\chi_G)$ consists of a cube with $\chi_G = 1$. The center of mass of the cube is the point $\underline{x}^* = (1{\cdot}8, 0, 0)^{\mathrm{T}} \in \mathbb{R}^3$, the largest sphere contained in the cube has a radius equal to 0·65, and the facets of the cube are parallel to the Cartesian coordinate planes (see Fig. 1 b)). Figure 2 shows $(\Omega;\chi)$ and $(\Omega_G;\chi_G)$ together. Remember that, in the scattering phenomena studied here, $\Omega$ and $\Omega_G$ are not present together in $\mathbb{R}^3$, as shown Fig. 2. In fact, $\Omega_G$ is only a "ghost".

First, we show the quantitative character of the series expansion. We have chosen $\lambda = 0{\cdot}999$, $\epsilon = 1{\cdot}7$ and the incident wave as in formula (100) with $\underline{\gamma} = (1, 0, 0)^T$, $q = 1$ and $S = 5$.

Figures 3 and 4 show the wave scattered by the active obstacle $u_a^s$ on the surface of the sphere with center at the origin and radius 3, i.e., on $\partial B_3$, when the optimal-control input is used, along with the wave scattered by the passive obstacle $u_p^s$, and the wave scattered by the ghost $u_G^s$. Note that $\Omega_\epsilon = B_{2{\cdot}7}$, so that $\Omega_\epsilon \subset B_3$. We have represented the convolution of $u_a^s, u_p^s, u_G^s$ with $\check{I}_K$ (Fig. 3) and with $\check{I}_{\mathbb{R}\setminus K}$ (Fig. 4), respectively, in a color map for three values of the time variable $t$, that is, $t = 1$, $t = 3{\cdot}5$ and $t = 5{\cdot}5$. We have chosen these three values of $t$ since they characterize three different situations that distinguish the passive and the smart obstacle. Note that the incident acoustic wave packet comes from the negative $x_1$-axis and hits first $\Omega$ and later $\Omega_G$ if we think of the ghost $\Omega_G$ as a real scatterer. That is, the passive obstacle must react before the ghost obstacle. In fact, when $t = 1$, the passive obstacle generates a measurable scattered wave, while the ghost obstacle does not irradiate substantial energy. When $t = 3{\cdot}5$, the situation is reversed since the incoming field has left the passive obstacle but its tail is still touching the ghost obstacle (if we think of the ghost as a real scatterer).

The first qualitative result shown in Figs. 3 and 4 shows the effect produced by the solution of the optimal-control problem (1), (4)–(6), (10). In fact, in Fig. 3 we can see that $\check{I}_K * u_a^s$ (see column 2) resembles $\check{I}_K * u_G^s$ (see column 3), and we can also see how different the field $\check{I}_K * u_p^s$ (see column 1) is from $\check{I}_K * u_a^s$ (see column 2). That is, on the surface $\partial B_3$, the field generated by the smart obstacle resembles the field generated by the ghost obstacle on the band $K$, this is, the definite-band ghost-obstacle effect. In Fig. 4, columns 1 and 2 are similar and different from column 3. That is, in Fig. 4 we can see that, outside the band $K$, the active obstacle reacts as the passive obstacle: there is no ghost effect.

We now show the quantitative character of the series expansions (94) and (95). The obstacle $(\Omega;\chi)$ and the ghost obstacle $(\Omega_G;\chi_G)$ and the other parameters defining the experiment are same as those chosen in the second experiment. We show the quantitative character of the series expansions defining $\tilde{u}^*_{\omega,\underline{\alpha},\sigma,l,m}$ and $\tilde{v}^*_{\omega,\underline{\alpha},\sigma,l,m}$ in (96) and (97). Let us denote by $\tilde{u}_{S,\omega,\underline{\alpha},\sigma,l,m}$ and $\tilde{v}^*_{S,\omega,\underline{\alpha},\sigma,l,m}$ the series expansions given in (96)

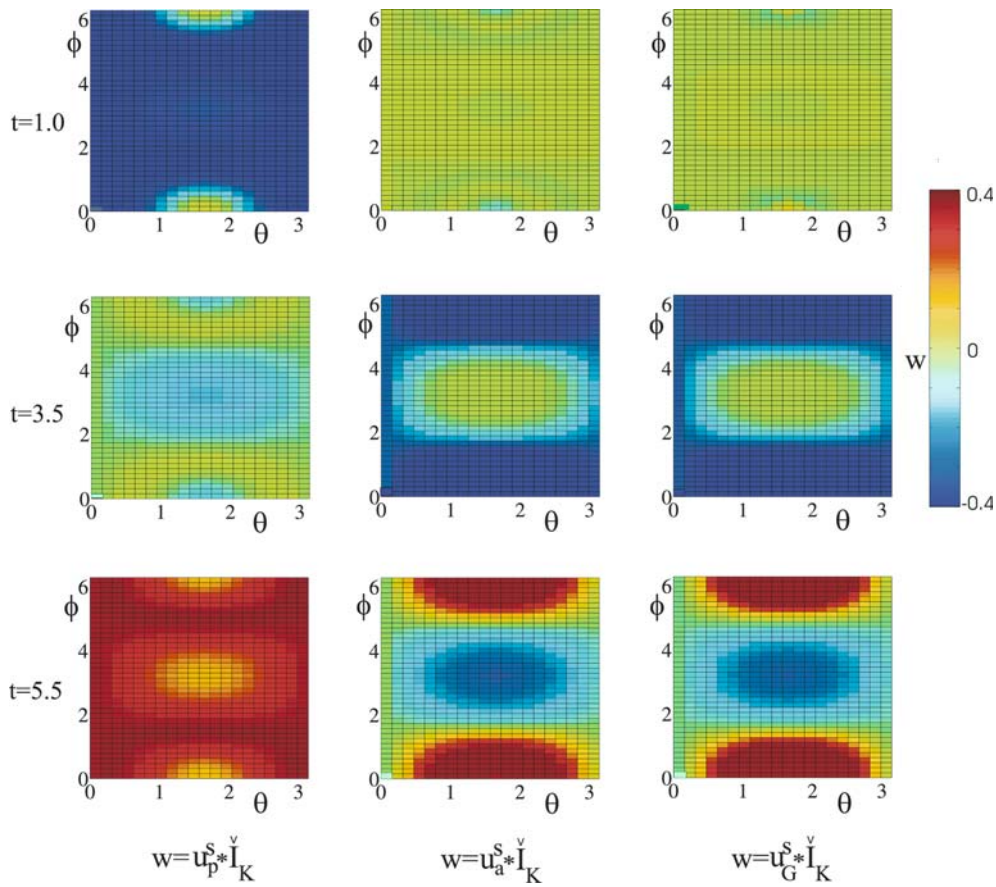


**Fig. 3** Comparison on the definite band $K$ at three different time values of the field scattered by the passive obstacle (column 1), by the active obstacle (column 2) and by the ghost obstacle (column 3)

and (97), respectively, truncated at $s = S$, and let us define the following quantities:

$$\varepsilon_{u^s}^S = \frac{\left[\sum_{\sigma=0}^{1}\sum_{l=\sigma}^{L_{\max}}\sum_{m=\sigma}^{l}|\tilde{u}_{S,\omega,\underline{\gamma},\sigma,l,m}|^2\right]^{1/2}}{\sum_{\sigma=0}^{1}\sum_{l=\sigma}^{L_{\max}}\left[\sum_{m=\sigma}^{l}|\sum_{s=0}^{S}\tilde{u}_{s,\omega,\underline{\gamma},\sigma,l,m}|^2\right]^{1/2}}, \tag{108}$$

and

$$\varepsilon_{\varphi}^S = \frac{\left[\sum_{\sigma=0}^{1}\sum_{l=\sigma}^{L_{\max}}\sum_{m=\sigma}^{l}|\tilde{v}^*_{S,\omega,\underline{\gamma},\sigma,l,m}|^2\right]^{1/2}}{\left[\sum_{\sigma=0}^{1}\sum_{l=\sigma}^{L_{\max}}\sum_{m=\sigma}^{l}|\sum_{s=0}^{S}\tilde{v}^*_{s,\omega,\underline{\gamma},\sigma,l,m}|^2\right]^{1/2}}. \tag{109}$$

In Table 3, we show the behavior of $\varepsilon_{u_s}^S, \varepsilon_{\varphi}^S$ when $S = 1, 2, \ldots, 8$, $L_{\max} = 16$ and $\omega/c = 0{\cdot}5,\ 1,\ 2,\ 3, \lambda = 0{\cdot}999$, $\mu = 0{\cdot}001$, $K = (-3, 3)$. Table 3 shows that the formal series expansions in powers of $(\omega/c)(\xi - 1)$ used in this experiment are numerically convergent when $(\omega/c)\max_{\underline{\hat{x}}\in\partial B}|\xi(\underline{\hat{x}}) - 1|$ is not large. A detailed discussion of the convergence of such series expansions can be found in [1].

We conclude this section by showing Table 4, which is similar to Table 1 but pertains to the definite-band ghost-obstacle problem. Let $t_\nu = 1 + 0{\cdot}5(\nu - 1)$, $\nu = 1, 2, \ldots, 10$ and $R_i = 3 + 0{\cdot}5(i - 1)$, $i = 1, 2, \ldots, 5$, we introduce three quantities analogous to $i_{F,K}$, $\tilde{i}_{F,K}$ and $\check{i}_{F,K}$ that we denote by $i_{G,K}$, $\tilde{i}_{G,K}$, $\check{i}_{G,K}$. Let $u_a^s$ be the wave scattered by the smart-obstacle solution of the optimal-control problem (1), (4)–(6), (10). We define

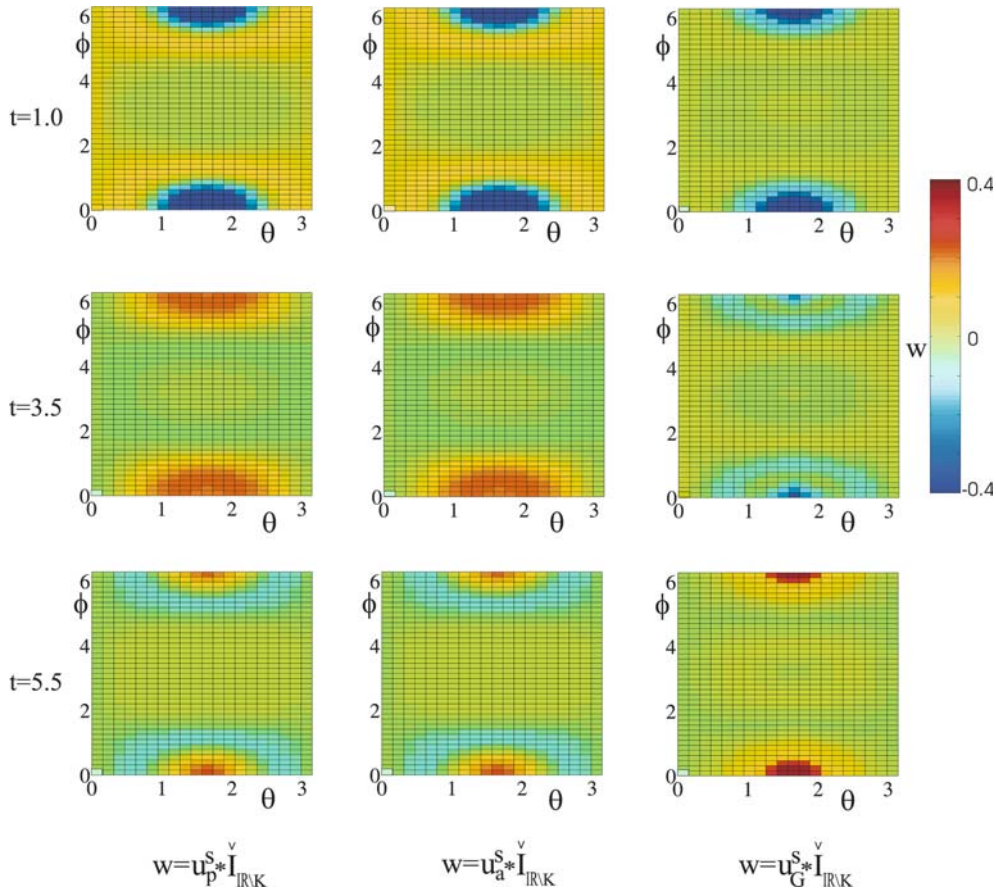


**Fig. 4** Comparison of the field scattered by the passive obstacle (column 1), by the active obstacle (column 2) and by the ghost obstacle (column 3) outside the definite band $K$ at three different time values

**Table 4** Experiment 2: $\Omega = B_{1\cdot02}$, $\chi = 1$, $\Omega_G$= cube (see Figs. 1b and 2) $\chi_G = 1$, incident wave (100) with $q = 1$

| $K$ | $i_{G,K}$ | $\tilde{i}_{G,K}$ | $C_{\psi,K}$ | $\tilde{i}_{G,K}/C_{\psi,K}$ | $\check{i}_{G,\mathbb{R}\setminus K}$ |
|---|---|---|---|---|---|
| $\lambda = 0\cdot5, \mu = 0\cdot5, \varsigma = 1$ | | | | | |
| $(-0\cdot5, 0\cdot5)$ | 0·527656 | 0·59577 | $3\cdot96336\times10^{-2}$ | 15·0379 | $4\cdot0311\times10^{-8}$ |
| $(-1, 1)$ | 0·42748 | 0·48462 | 0·31894 | 1·51947 | $2\cdot06139\times10^{-8}$ |
| $(-3, 3)$ | $2\cdot7960\times10^{-2}$ | 0·29143 | 0·771074 | 0·37795 | $2\cdot06159\times10^{-8}$ |
| $\mathbb{R}$ | $3\cdot8218\times10^{-2}$ | 0·29827 | 0·77377 | 0·385476 | 0 |
| $\lambda = 0\cdot999, \mu = 0\cdot001, \varsigma = 1$ | | | | | |
| $(-0\cdot5, 0\cdot5)$ | 0·606725 | 0·70988 | 5·81541 | $1\cdot2207\times10^{-1}$ | $4\cdot0311\times10^{-8}$ |
| $(-1, 1)$ | 0·617477 | 0·66329 | 41·9809 | $1\cdot5710\times10^{-2}$ | $2\cdot06139\times10^{-8}$ |
| $(-3, 3)$ | 0·440303 | 0·64878 | 69·1558 | $9\cdot3814\times10^{-3}$ | $2\cdot06159\times10^{-8}$ |
| $\mathbb{R}$ | 0·418560 | 0·65770 | 69·2068 | $9\cdot5034\times10^{-3}$ | 0 |

**Table 5** CPU time versus number of processors

| Processors | Seconds |
|---|---|
| 8 | 692·09 |
| 16 | 309·68 |
| 32 | 186·10 |
| 64 | 107·19 |
| 128 | 54·25 |

for $\nu = 1,2,\ldots,10$ and $i = 1,2,\ldots,5$ the following quantities:

$$\epsilon^a_{G,K,i}(t_\nu) = \int_{\partial B_{R_i}} \left| \int_{\mathbb{R}} \mathrm{d}\tau \;\check{I}_K(\tau) \left( u^s_{a,L_{\max}}(\underline{x}, t_\nu - \tau) - u^s_{G,L_{\max}}(\underline{x}, t_\nu - \tau) \right) \right|^2 \mathrm{d}s_{\partial B_{R_i}}(\underline{x}), \tag{110}$$

$$\epsilon^p_{G,K,i}(t_\nu) = \int_{\partial B_{R_i}} \left| \int_{\mathbb{R}} \mathrm{d}\tau \;\check{I}_K(\tau) \left( u^s_{p,L_{\max}}(\underline{x}, t_\nu - \tau) - u^s_{G,L_{\max}}(\underline{x}, t_\nu - \tau) \right) \right|^2 \mathrm{d}s_{\partial B_{R_i}}(\underline{x}), \tag{111}$$

and finally

$$i_{G,K} = \min_{\substack{\nu = 1,2,\ldots,10,\\ i = 1,2,\ldots,5}} \frac{|\epsilon^p_{G,K,i}(t_\nu) - \epsilon^a_{G,K,i}(t_\nu)|}{\epsilon^p_{G,K,i}(t_\nu)}, \tag{112}$$

$$\tilde{i}_{G,K} = \frac{1}{50} \sum_{\nu=1}^{10} \sum_{i=1}^{5} \left\{ \frac{|\epsilon^p_{G,K,i}(t_\nu) - \epsilon^a_{G,K,i}(t_\nu)|}{\epsilon^p_{G,K,i}(t_\nu)} \right\}. \tag{113}$$

Table 4 shows the behavior of these quantities for $S = 5$, $q = 1$. The results shown in Table 4 confirm the analysis made previously for the definite-band furtivity problem.

Table 5 shows the execution time required to compute (once) the quantities $\sum_{s=0}^{S} \tilde{u}_{s,\omega,\underline{\gamma},\sigma,l,m}$ and the quantities $\sum_{s=0}^{S} \tilde{v}^*_{s,\omega,\underline{\gamma},\sigma,l,m}$, $\omega = \omega_i, i = 1,2,\ldots,N_1, \sigma = 0,1, l = \sigma,\sigma+1,\ldots,L_{\max}, m = \sigma,\sigma+1,\ldots,l$. Note that re-summing these quantities as in (94), (95), and (52), (53) we can compute the approximations to the solutions $u^s_a$ and $\varphi$ of the optimal-control problem (1), (4–6), (10) in every point $(\underline{x}, t) \in (\mathbb{R}^3 \setminus \Omega) \times \mathbb{R}$. We recall that we have chosen $S = 5$, $N_1 = 400$, $L_{\max} = 16$ and $K = (-3,3)$. The execution time is measured using the function `MPI_WTIME()` that returns a floating-point number representing the elapsed wall-clock time since some chosen time in the past measured in seconds.

We note that passing from 8 to 32 processors, the time is reduced by a factor of about 3·72, so that the speed-up factor is $3{\cdot}72/4 = 0{\cdot}93$. Similarly, going from 8 to 64 processors, the speed up factor is $6{\cdot}46/8 \approx 0{\cdot}80$ and going from 8 to 128 is $12{\cdot}75/16 \approx 0{\cdot}79$. This speed-up is really impressive.

## 5 Conclusions

In this paper we have studied smart obstacles that pursue the goal of being undetectable or of appearing in a location different from their actual location when hit by an incoming time-dependent wave composed of time-harmonic components with frequencies in a given band. We modeled the direct scattering problems involving these smart obstacles as optimal-control problems for the wave equation (see (1), (4)–(6), (10)), and we derived the first-order optimality condition (15)–(24) associated with these control problems using the Pontryagin maximum principle. Finally, we developed a highly parallelizable numerical method to solve the equation set (15)–(24). The most usual numerical solvers for optimal-control problems for systems described by partial differential equations are iterative schemes that require the solution of one or

several direct problems, that is, problems involving the partial differential equations, at each iteration. The method proposed here is not iterative and obtains the solution of the optimal-control problem (1), (4)–(6), (10) solving the exterior problem defined by equations (15)–(24). This means solving only one problem involving partial differential equations. The exterior problem (15)–(24) can be solved efficiently using the operator-expansion method. In fact, proceeding as in [1, 11], we can reduce the solution of this exterior problem to the solution of a set of systems of integral equations (66), (67). When simple obstacles and incident waves of sufficiently low frequency are considered, these equations can be solved using spherical harmonic functions to represent the data, the integral kernels and the unknown densities. In particular, owing to the use of the expansions (75), (76), the solution of the systems of integral equations (66), (67) is reduced to the solution of diagonal systems of linear equations. The method proposed here is very well suited for parallel computing; in fact, the most demanding part of the computation, which is the computation of the coefficients of the expansions in spherical harmonic functions of the data and of the integral kernels, can be done in parallel giving an impressive speed-up factor. The main restriction of the proposed method is that the shape of the obstacles must be simple, that is, not too far from being spherical and that the incident time-harmonic waves must have a sufficiently low frequency. This restriction is necessary since we want to use a sphere with its center in the origin and radius one as base point of the expansions (75), (76) and the spherical harmonic functions as basis to represent the data and the unknowns of the integral equations. Work is in progress to overcome this restriction by introducing new base points for the expansions (75), (76) and new function bases to discretize the integral equations coming from the new expansions. The function bases must be able to discretize the integral equations obtained from the expansions with linear systems similar to diagonal systems, that is, systems with a very sparse coefficient matrix. We can conclude that the mathematical models proposed to study the scattering problems involving smart obstacles are valid and that the numerical method we proposed to solve these models is a valuable tool in the quantitative solution of scattering problems involving smart obstacles.

## References


1. Mariani F, Recchioni MC, Zirilli F (2001) The use of the Pontryagin maximum principle in a furtivity problem in time-dependent acoustic obstacle scattering. Waves Random Media 11:549–575
2. Fatone L, Recchioni MC, Zirilli F (2003) Some control problems for the Maxwell equations related to furtivity and masking problems in electromagnetic obstacle scattering. In: Cohen GC, Heikkola E, Joly P, Neittaanmaki P (eds) Mathematical and numerical aspects of wave propagation. Waves 2003. Springer Verlag, Berlin, pp 189–194
3. Fatone L, Recchioni MC, Zirilli F (2004) Furtivity and masking problems in time dependent electromagnetic obstacle scattering. J Optimiz Theory Appl 121:223–257
4. Fatone L, Recchioni MC, Zirilli F (2004) A masking problem in time dependent acoustic obstacle scattering. ARLO – Acoust Res Lett Online 5(2):25–30
5. Fatone L, Recchioni MC, Zirilli F (2005) Mathematical models of "active" obstacles in acoustic scattering. In: Cagnol J, Zolesio JP (eds) Control and boundary analysis. Lecture Notes in Pure and Applied Mathematics vol 240. Marcel Dekker/CRC Press Boca Raton, Fl. USA. pp 119–129
6. Chambers B (1999) A smart radar absorber. J Smart Mater Struct 8:64–72
7. Ford KL, Chambers B (2000) A smart microwave absorber. IEE Electron Lett 36:50–52
8. Chambers B, Tennant A (2002) General analysis of the phase-switched screen Part 1: The single layer case. Proc IEE Part F – Radar Sonar Navig 149:243–247
9. Chambers B, Tennant A (2002) Influence of switching waveform characteristics on the performance of a single layer phase-switched. IEEE Trans Electromagn Compat 44:434–441
10. Nečas J (1967) Les méthodes directes en théorie des équations elliptiques. Masson & Cie. Publ, Paris
11. Mecocci E, Misici L, Recchioni MC, Zirilli F (2000) A new formalism for time dependent wave scattering from a bounded obstacle. J Acoust Soc Am 107: 1825–1840
12. Colton D, Kress R (1983) Integral equation methods in scattering theory. J. Wiley & Sons, New York
13. Knowles G (1981) An introduction to applied control. New York, Academic Press
14. Lions JL (1971) Optimal control of systems governed by partial differential equations. Springer Verlag, Berlin
15. Balakrishnan AV (1976) Applied functional analysis. Springer Verlag New York
16. Milder DM (1991) An improved formalism for wave scattering from rough surface. J Acoust Soc Amer 89:529–541

17. Milder DM (1996) Role of the admittance operator in rough-surface scattering. J Acoust Soc Amer 100:759–768
18. Milder DM (1996) An improved formalism for electromagnetic scattering from a perfectly conducting rough surface. Radio Sci 31:1369–1376
19. Smith RA (1996) The operator expansion formalism for electromagnetic scattering from rough dielectric surfaces. Radio Sci 31:1377–1385
20. Milder DM (1998) An improved formulation of coherent forward scatterer from random rough surfaces. Waves Random Media 8:67–78
21. Piccolo S, Recchioni MC, Zirilli F (1996) The time harmonic electromagnetic field in a disturbed half-space: an existence theorem and a computational method. J Math Phys 37:2762–2786
22. Misici L, Pacelli G, Zirilli F (1998) A new formalism for wave scattering from a bounded obstacle. J Acoust Soc Amer 103:106–113
23. Fatone L, Pignotti C, Recchioni MC, Zirilli F (1999) Time harmonic electromagnetic scattering from a bounded obstacle: an existence theorem and a computational methods. J Math Phys 40:4859–4887
24. Mariani F, Recchioni MC, Zirilli F (2002) A perturbative approach to acoustic scattering from a vibrating bounded obstacle. J Comput Acoust 10:349–384
25. Mayne DQ, Michalska H (1990) Receding horizon control of nonlinear systems. IEEE Trans Autom Control 35:814–824
26. Michalska H, Mayne DQ (1993) Robust receding horizon control of constrained nonlinear systems. IEEE Trans Autom Control 38:1623–1633
27. De Nicolao G, Magni L, Scattolini R (1998) Stabilizing receding-horizon control of nonlinear time-varying systems. IEEE Trans Autom Control 43:1030–1036
28. Armaou A, Christofides PD (2002) Dynamic optimization of dissipative PDE systems using nonlinear order reduction. Chem Enging Sci 57:5083–5114
29. Bendersky F, Christofides PD (2000) Optimization of transport-reaction processes using nonlinear model reduction. Chem Enging Sci 55:4349–4366
30. Recchioni MC, Zirilli F (2003) The use of wavelets in the operator expansion method for time dependent acoustic obstacle scattering. Siam J Sci Comput 25:1158–1186
31. Pontryagin LS, Boltiamskii VG, Gamkrelidze RV, Mischenico F (1974) Théorie mathématique des processus optimaux. Editions Mir Moscou
32. Yosida K (1995) Functional analysis. Springer Verlag, Berlin
33. Colton D, Kress R (1992) Inverse acoustic and electromagnetic scattering theory. Springer Verlag, Berlin